Habitable Planet, 2025, 1(1&2):197–220

Habitable Planet

Journal Homepage: www.habitableplanetjournal.com

Archean crustal evolution and building of habitable continents: Insights from the Western Dharwar Craton

K.R. Aadhiseshan and M. Jayananda*

School of Natural Sciences and Engineering, National Institute of Advanced Studies, IISc Campus, Bengaluru – 560012, India

ABSTRACT

This contribution presents a comprehensive review synthesis addressing Archean crustal evolution, redox conditions of surface environments, oxygenation of ocean and microbial activity leading to building the habitable continent in the western Dharwar craton (WDC). The WDC preserve ca. 3600–2600 Ma crustal record comprising TTG-type granitoids, volcanic-sedimentary greenstone sequences and potassic granite plutons. Tectonic fabrics mapping in the WDC reveal classical dome-keel patterns bordered by widely spaced regional shear zones network with progressive increase of metamorphic grade from north to south. U–Pb zircon ages and Sm–Nd whole rock isochrons suggest successive stages crust formation which contribute to episodic continental growth during ca. 3450–3350 Ma, 3300–3200 Ma, ca. 3230–3150 Ma, ca. 3000–2900 Ma, 2700–2600 Ma with spatially associated crustal reworking events ca. 3150 Ma, ca. 3000–2950 Ma, 2600 Ma and ca. 2500 Ma leading to stabilization of crust. Elemental and Nd isotope data of ca. 3400–3150 Ma greenstone volcanics reveal their derivation from primitive to deep mantle reservoirs in plume setting whilst ca. 3000–2900 Ma volcanism originated in shallower heterogeneous mantle caused by asthenosphere upwelling. On the other hand, ca. 2700–2600 Ma volcanics generated by melting of depleted to enriched arc mantle. Distinct lithologic assemblages, combined with U–Pb zircon ages, elemental and isotopes (whole rock Nd and zircon *in-situ* Hf) suggest that oldest cratonic core formed by assembly of ca. 3600–3500 Ma ancient microcontinental remnants, 3400–3300 Ma oceanic plateau fragments, oceanic arcs and ocean ridge through horizontal motion close to 3200 Ma. Magmatic records and documented strain suggest vertical motions are dominant tectonic mode prior to ca. 3400 Ma whilst horizontal motion initiated ca. 3350 Ma onwards leading to building of oceanic arcs with subsequent collision of diverse tectonic elements with eventual slab breakoff leading to mantle upwelling, lower crustal melting, caused gravitational collapse of high density supracrustal load forming keels with rise of low density infracrustal granitoids resulting in domes. Tectonic fabric analysis of ca. 3000–2850 Ma intracratonic basins developed on the stabilized continental crust through sagduction controlled by emplacement of dense volcanic traps on the basement. Finally, geological framework and structural patterns of the ca. 2700–2600 Ma greenstone basins point to arc settings. Collision of arcs with eventual slab breakoff leads to generation and emplacement of Chitradurga–Arsikere–Banavara potassic plutons in the basement or in between the volcanic arcs.

Redox sensitive elements and isotope biomarkers (Fe, N and Mass Independent Fractionation-Sulphur isotopes) data on the sedimentary record reveal dominantly anoxic environments during ca. 3400–3000 Ma whilst ca. 3000 Ma onwards a shift from anoxic to minimum oxygen on ocean surface with periodic organic production linked to the microbial activity and oxygenation building of habitable continent a few hundred million years prior to the Great Oxidation Event (GOE).

ARTICLE INFO

History:
Received Jun 04, 2025
Revised Jul 03, 2025
Accepted Jul 03, 2025

Keywords:
Archean
Dharwar craton
Habitable continent
Microbial activity
Redox conditions

Citation:
Aadhiseshan, K.R., Jayananda, M. 2025. Archean crustal evolution and building of habitable continents: Insights from the Western Dharwar Craton. Habitable Planet 1(1&2), 197–220. https://doi.org/10.63335/j.hp.2025.0016.

*Corresponding author. Email: mjayan.geol@nias.res.in (MJ)

Research highlights

- Archean continental crust formed in successive stages as granitoid–greenstone assemblages in plume-arc settings.
- Archean continental crust involved in reworking leading to emplacement of potassic plutons and cratonization.
- Redox sensitive elements and isotope biomarkers reveal anoxic environments with periodic fluctuations in oxygen availability on ocean surface during Meso-to-Neoarchean.
- Redox evolution of ocean-atmospheric system of early earth controlled by microbial activity and oxygenation of ocean-atmosphere initiated a few hundred million years before the GOE.

1 Introduction

Understanding processes involved in building-up of habitable continents as well as redox evolution of ocean-atmosphere system are major focal themes of research in Earth and Planetary Sciences. The time frame and processes involved in the formation of habitable continents and evolution of oxygenated environments is a prerequisite for predicting the long-term future changes in human living conditions particularly in the context of global climate change. The Archean cratonic assemblages worldwide form important archives for our understanding the evolution of habitable continents, mantle, oceans, atmosphere, life and evolving tectonics of the early earth.

In recent years numerous studies focused on the preserved Archean continental fragments in Southern Africa (Kaapvaal), SW Greenland, Western Australia (Pilbara and Yilgarn), Canada (Superior and Slave provinces), South America (Sao Francisco and Amazonian craton), Peninsular India (Singhbhum and Dharwar), China (North China Craton) through multidisciplinary approach which greatly contributed to our understanding of the fundamental architecture of cratons, early earth dynamics including onset of plate tectonics, building of habitable continents and surface environments. Despite numerous studies, the thematic issues of early earth dynamics including the timing of onset of horizontal motion of plates, oxygenation of ocean and atmosphere are still the subjects of much discussion. A much-debated issue related to the tectonics of the Archean earth particularly focusing vertical versus horizontal motions (Bedard, 2018; Wyman, 2018). Furthermore, timing of initiation of plate tectonics also subject of much discussion wherein most workers agree that horizontal motion of tectonic plates initiated close to ca. 3300 Ma (Jayananda et al., 2023 and references therein) whilst others argued the horizontal tectonics initiated very early in the history of the planet earth (e.g., Komiya et al., 2015). The interplay of geological, chemical, microbial activity and tectonic processes in building of habitable continents, redox conditions of surface environments, metabolic pathways of biologic activity and early habitats on Archean earth is also subject of much lively discussions (e.g., Reinhard and Planavsky, 2020). Redox sensitive elements and isotope markers reveal the Great Oxygenation Event (GOE) close to ca. 2400 Ma (Bekker et al., 2004) whilst some workers argue that oxygenation of oceans occur a few hundred million years prior to GOE (e.g. Anbar et al., 2007). Therefore, it is important to address the key issues related to evolving early earth including geodynamic processes involved in building habitable continents, oxygenation of oceans, microbial activity and emergence of biosphere. Archean TTGs are most voluminous rocks in the cratons across the world and represent first differentiated continental crust from the mantle. Archean greenstone volcanism is the dynamic expression of thermal structure and chemical composition of the contemporaneous mantle. Archean sedimentary sequences form critical windows for early Earth's atmosphere, surface environments, crust-hydrosphere interactions and biosphere. These sedimentary sequences preserve record of redox conditions ocean-atmospheric system, shift from anoxic to oxygenated environments and origin of life. Despite numerous studies addressed early earth evolution including tectonics of the Archean earth, building of habitable continents and oxygenation of ocean-atmospheric system are the subjects of much discussion and lively debates. In this context the western Dharwar craton, southern India form a key region to address the early earth dynamics and building of habitable continents as the oblique crustal panel display a large section of tilted Archean crustal section showcasing upper to lower crust forming a wide time and tectonic window into Archean earth (Chardon et al., 2011; Jayananda et al., 2018, 2023). Consequently, the main purpose of this contribution is to present a comprehensive review addressing timing and mechanisms of juvenile crust accretion as well as reworking processes, sedimentary environments, oxygenation of oceans and emergence of biosphere and building of habitable continent.

2 Tectono-stratigraphic framework of the Dharwar craton

The Dharwar craton showcases three-dimensional architecture of Archean crust with well-preserved granitoid–greenstone assemblages forming key archives for study of the early earth. The craton comprises voluminous granitoids of diverse compositional types (TTGs, Transitional TTGs, potassic granites and sanukitoids), volcanic-sedimentary greenstone assemblages. Recent multidisciplinary research involving strain fabrics analysis, metamorphic records, isotope ages on the Dharwar craton reveal three distinct crustal blocks (Fig. 1—western, central and eastern) with independent crustal histories (Jayananda et al., 2013, 2018). The western block contains voluminous 3600–3200 Ma TTG-type granitoids and two distinct volcanic-sedimentary sequences comprising ca. 3400–3150 Ma Sargur Group and 3000–2600 Ma Dharwar Supergroup (Jayananda et al., 2018 and references therein). On the other hand, the Central block contains large remnants of older basement (3360–3150 Ma TTGs and remnants of high grade supracrustal units), voluminous 2700–2600 Ma Transitional TTGs, juvenile 2560–2520 Ma granitoids of sanukitoid affinity and minor ca. 2510 anatectic granite (Jayananda et al., 2018). The Eastern block comprises 2600–2550 Ma transitional TTGs, minor 2540–2530 sanukitoids and abundant 2535–2520 Ma diatexites (Jayananda et al., 2020). All the three crustal blocks assembled through westward converge of hot orogenic crust during 2560–2500 Ma (Chardon et al., 2011).

3 Geology of the Western Dharwar Craton (WDC)

The WDC (see Fig. 1) contain abundant volcanic-sedimentary basins which are surrounded by voluminous ca. 3600–3200 Ma TTG-type granitoids. The volcanic-sedimentary greenstone sequences were stratigraphically divided into older ca. 3400–3150 Ga Sargur Group and younger ca. 3000–2605 Ma Dharwar Supergroup. The older Sargur Group greenstone sequences found as narrow belts displaying tectonized contacts with adjacent TTG-type granitoids (Fig. 2a–d). They comprise volcanics of dominant komatiite lineage with minor basaltic to felsic pyroclastic flows. These volcanic sequences interlayered sedimentary units like quartzite-pelite-carbonate-BIFs (Swami Nath and Ramakrishnan, 1981). Detrital zircons from sedimentary record reveal ca. 3600–3200 Ma (Harshitha et al., 2024). On the contrary the Dharwar Supergroup further subdivided into older (ca. 3000–2720 Ma) Bababudan Group and younger ca. 2740–2605 Ma Chitradurga Group (Swami Nath and Ramakrishnan, 1981). The Bababudan Group corresponds to intracratonic volcano-sedimentary basins which unconformably overlies the old basement with a paleosol at basement-cover contact (Chadwick et al., 1985). Stratigraphically Bababudan Group greenstone basin (Fig. 3a–d) starts with a paleosol at the uncoformable contact between the basement and oligomict conglomerate followed by thick vesicular to amygdaloidal basaltic flows with intermittent quartzite layers (often cross-bedded), phyllite, tuffs, felsic pyroclastic flows and thick BIFs occupying summits (Chadwick et al., 1985). Strain fabric trajectories, kinematic indicators and superimposed deformation patterns of Bababudan type locality reveal that high density greenstones have undergone a radial converging downward flow (sagduction-gravity sinking) with respect to its low density TTG basement (Chardon et al., 1998). The results of strain fabrics mapping and kinematic analysis from the Bababudan Group of greenstone basins (Chardon et al., 1998) coupled with structural evidence from other cratons (Zimbabwe and Pilbara) raise the possibility that a unique tectonic regime existed in the interior of the Archean cratons controlled by emplacement of dense volcanic traps, mantle underplating and thermal blanketing of continental crust.

The younger ca. 2740–2605 Ma Chitradurga Group (Kumar et al., 1996; Jayananda et al., 2013; Krapez et al., 2020) assemblages preserved in the type area of Chitradurga belt (Fig. 4a–d) and laterally stratigraphically equivalent Shimoga–Dharwar basin which laid on the older basement. These greenstone basins begin with polymictic conglomerates often show features of glaciomarine (Ojakangas et al., 2014) followed by thick basaltic flows, carbonate-greywacke-argillite sequences, tuffs, pyroclastic flows and BIFs. The sedimentary record includes different types of conglomerate like Talya polymict conglomerate along the western margin of Chitradurga basin reveal rapid dumping of detritus with different clasts sprinkled in clay to sand sized materials imply sedimentation in arc setting. The thick stromatolitic carbonates in the western part Chitradurga basin reveal shallow shelf environment whilst a thick sequence of greywackes, argillite, sulphide bearing carbonaceous shale and BIF to the east to NE imply deeper environment. The preserved sedimentary record in the Chitradurga basin suggests shallow to deep marine sub-oxic environments. Lithologic sequences coupled with detailed field based tectonic fabric analysis and elemental data reveal these younger volcanic-sedimentary basins developed in arc environments.

The Shimoga–Dharwar basin (Figs. 5a–d; 6a–d respectively) is the youngest volcanic-sedimentary sequences in the Dharwar craton corresponds to upper part of the Chitradurga Group. The Shimoga basin overlain on ca. 3200–3150 Ma Archean gneiss basement and comprises mafic volcanics with interlayered chert-carbonate-greywacke-argillite-BIFs and felsic pyroclastic flows. Mafic volcanics define Sm–Nd whole rock isochron age of 2638 ± 66 Ma (Giri et al., 2019) whilst the felsic pyroclastic flows from the upper stratigraphic levels provided U–Pb zircon age of 2605 ± 5 Ma (Nutman et al., 1996). Elemental

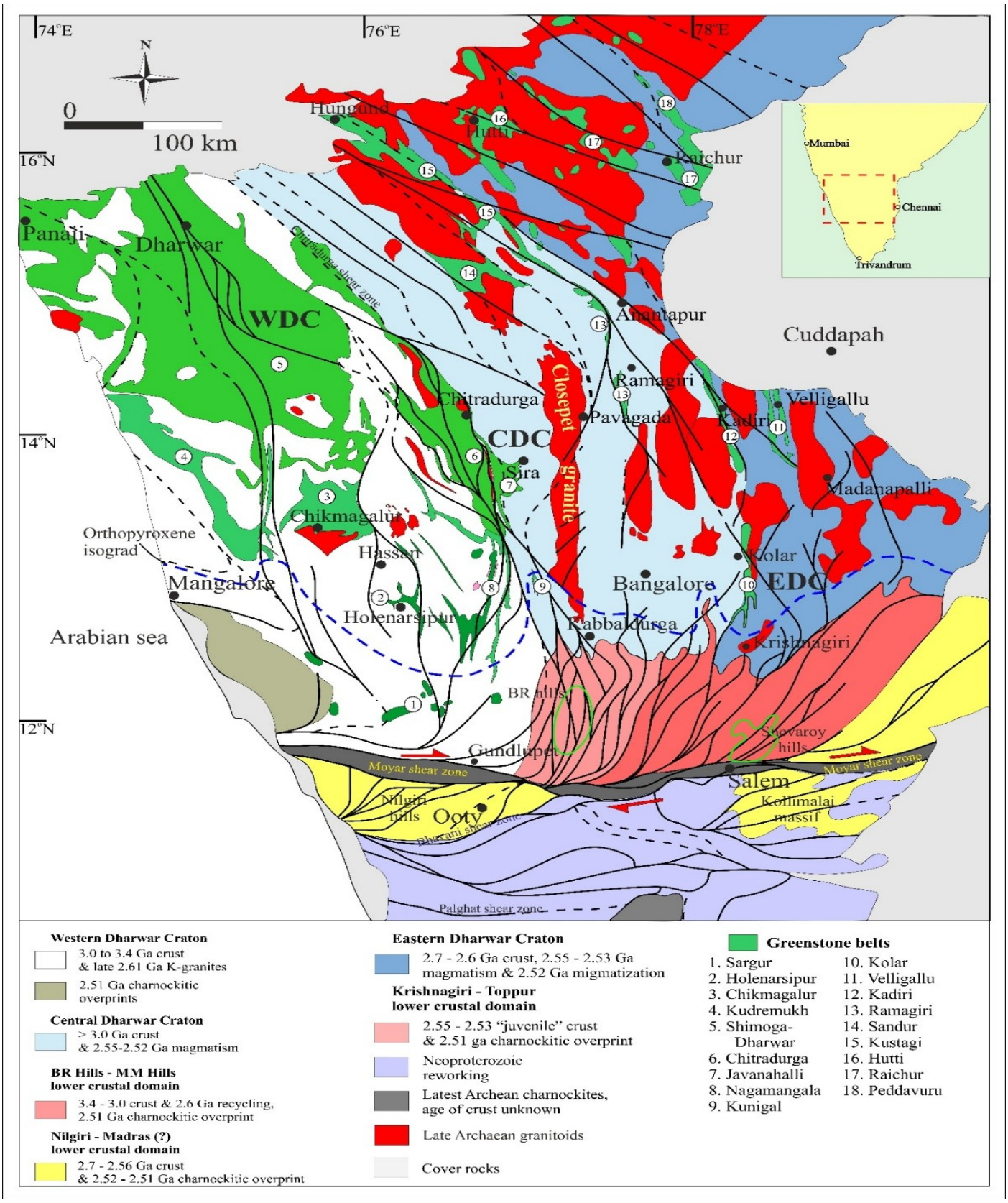

Fig. 1. Geological sketch map of the Dharwar craton, (after Jayananda et al., 2023).

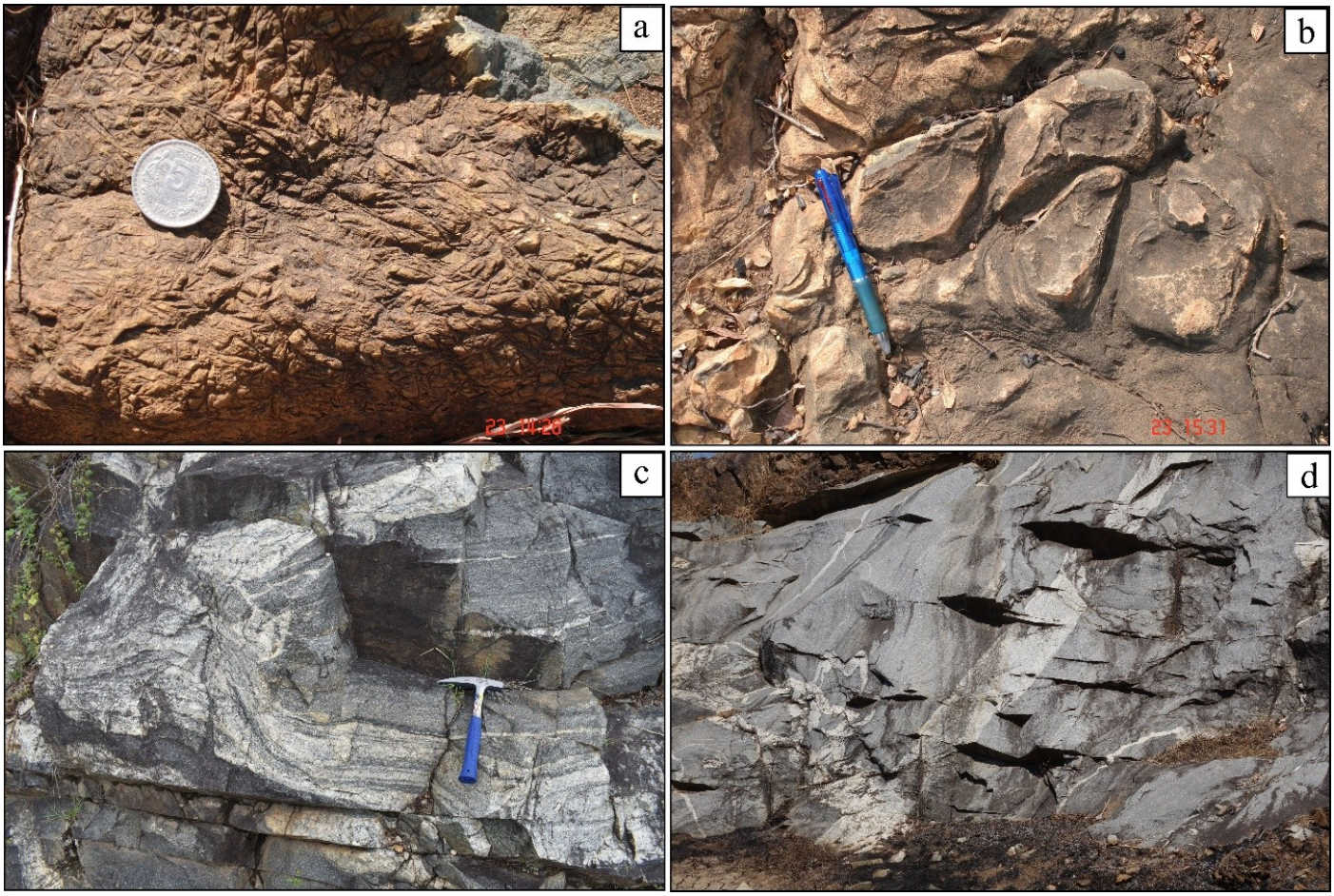

Fig. 2. (a) Spinifex textured komatiite from Banasandra greenstone belt about i.0 km NNW of Kunikenahalli; (b) pillowed komatiite from Banasandra near Kunikenahalli; (c) TTG type gneiss at an abandoned quarry at the base of the Bababudan basin about 5 km from Magadi hand post in Kalasapura road and (d) TTG type basement granitoid at an abandoned quarry at 19 km stone in Hassan-Gorur road.

data of the volcanic-sedimentary sequences attributed to continental arc setting. On the other hand, the Dharwar basin comprises minor mafic volcanics with most voluminous chert-carbonate-greywacke-argillite-BIFs sequences and felsic pyroclastic flows. Discrete granitoid intrusions found in the northern part of the Dharwar basin. No significant isotopic age data on the Dharwar basin is available except few U–Pb zircon ages two discrete plutons indicating ca. 2970–2950 Ma (Corfu and Hegde, 2020). Based on field based tectonic fabrics data, the Dharwar basin has been interpreted as a foreland basin (Chadwick et al., 2000).

Diverse granitoids are the most widespread rock assemblages in the WDC. These granitoids comprise several generations of different compositional types including TTGs, and potassic granites (Jayananda et al., 2018). The voluminous TTG-type granitoids forming the Archean basement which occur as weakly banded to migmatitic gneisses with alternate bands of leucocratic to mafic minerals. Strain field mapping and kinematic analysis on TTG-type gneisses reveal domal architecture in the Hassan–Gorur–Holenarsipur–J.C. Pura region forming the cratonal core of the WDC (Chardon et al., 2008; Jayananda et al., 2023). The ca. 3200 Ma diapiric trondhjemite intrudes the ca. 3400–3270 Ma TTGs-Sargur Group greenstone sequences and their emplacement was contemporaneous with the development of dome-keel structures (Jayananda et al., 2023). The ca. 3150 Ma granodioritic Chikmagalur pluton intrudes into the TTG basement both of which in turn form the basement for the ca. 3000–2850 Ma intracratonic Bababudan basin. Late potassic plutons intrude the basement and U–Pb zircon ages reveal two groups of potassic granites were emplaced during ca. 3000–2950 Ma and ca. 2640–2600 Ma (Jayananda et al., 2019). The Coorg block is separated from the WDC with the Mercara shear zone. Recent studies consider Coorg block as an exotic microcontinent formed during ca. 3300–3150 Ma with remnants of crust as old as Hadean and assembled with the

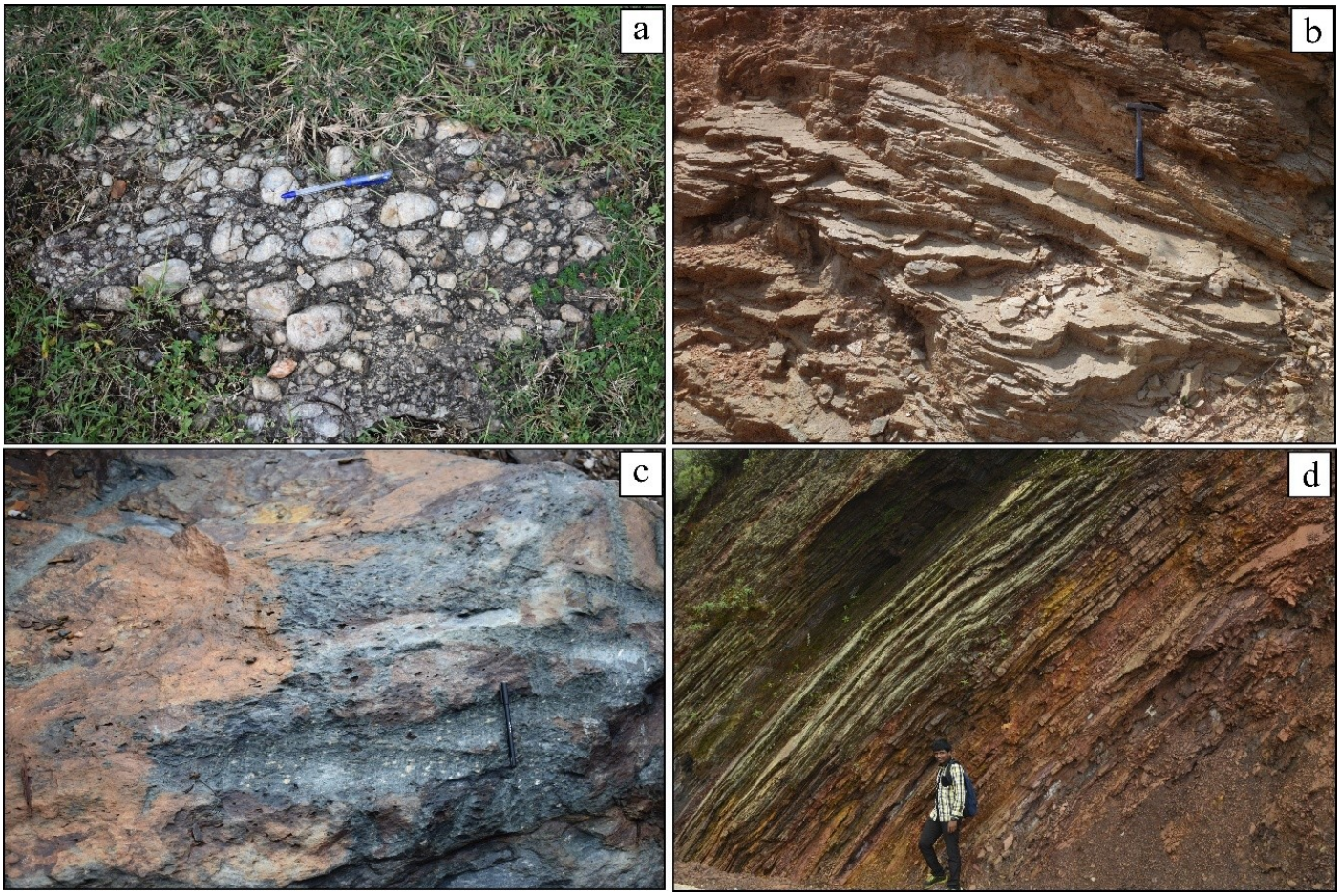

Fig. 3. (a) Oligomict conglomerate from the base of Bababudan basin at Karthikere road-cut in Belur–Chikmagalur road. (b) Mylonitic quartzite layer (decollement zone) at the Karthikere road cut. (c) Amygdular basalt from Kalasapura Formation about 4 km from Chikmagalur in Kadur road. (d) Banded Iron Formation at Kavikalgandi cross in the Bababudan hills.

western Dharwar craton during ca. 3100 Ma (Roberts and Santosh, 2018).

4 Structural patterns and cratonal architecture

On cratonal scale LANDSAT-TM data together with our field-based fabrics mapping reveal dome and basin patterns, north trending steep foliations, flat foliations and regional strike-slip shear zones (Chardon et al., 2008). The whole craton was affected by a major late Archaean shear deformation and green schist to granulite facies metamorphism that affected the whole Archaean crust. This event slightly preceded by the emplacement of the several N–S trending composite granitoid plutons including the large 500 km Closepet batholith and lower crustal flow in the central Dharwar craton (Chardon et al., 2011). The cratonal scale conjugate shear zone pattern results by interference between two shear systems, a NE trending dextral shear system in the south and sinistral WNW trending shear system in the north. The old lithosphere of western Dharwar craton underwent moderate shortening and strain localization along widely spaced shear zones (Chardon et al., 2008).

5 Regional metamorphism

Archean metamorphic record of the Dharwar craton and its spatial link to crust formation and tectonics is not well constrained. Earlier studies documented north to south progressive increase of metamorphic grade from greenschist in the north through unbroken amphibolite to granulite facies transition to the south which was attributed to northward tilt of the craton. The whole Archean crust in the Dharwar craton affected by ca. 2500 Ma regional metamorphism of granulite to greenschist facies (Jayananda et al., 2013). Subsequent studies have documented pre-2500 Ma metamorphic event in the western Dharwar craton close ca. 3100 Ma documented (Jayananda et al., 2013).

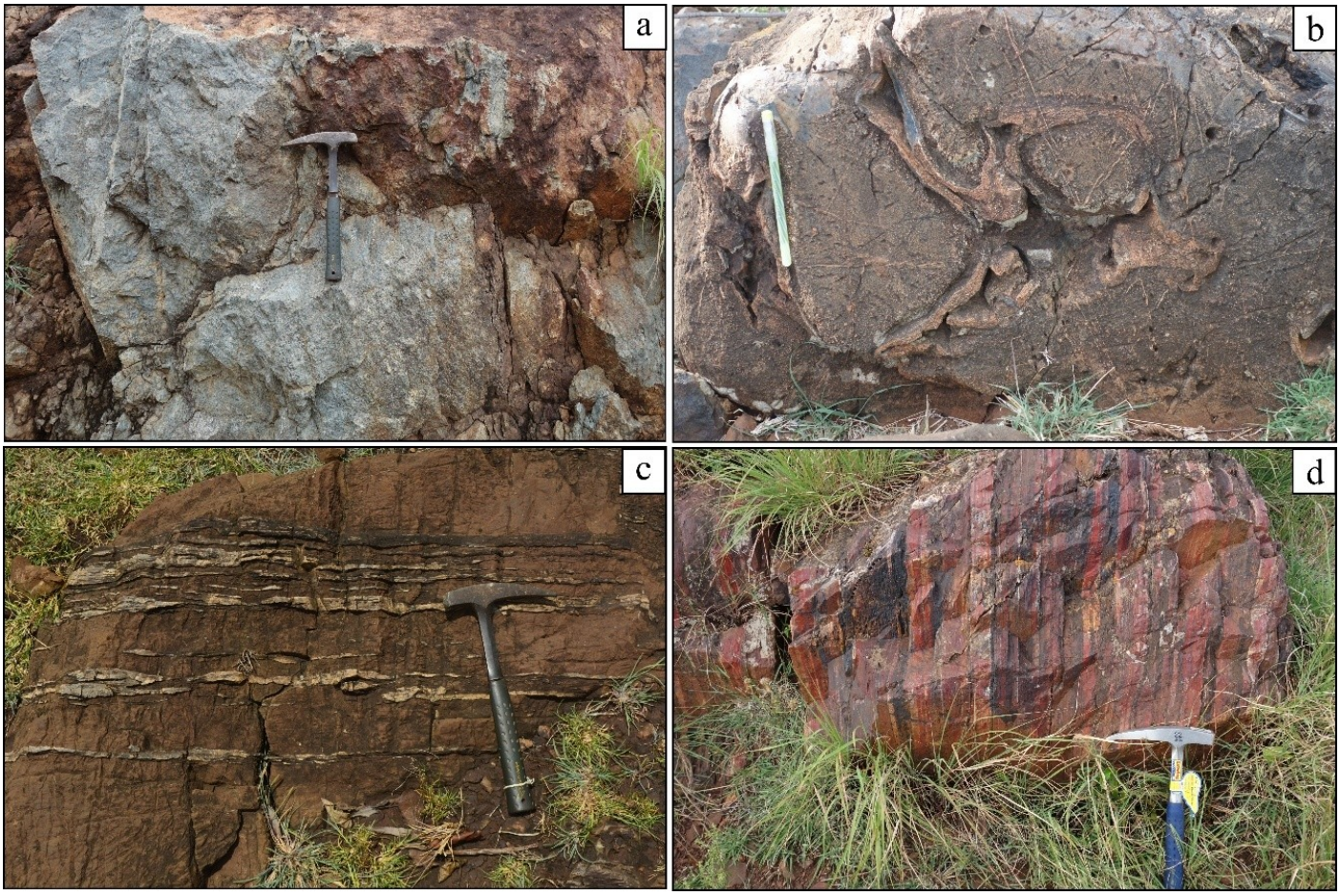

Fig. 4. (a) Massive basaltic flow about 4 km SSE of K.M. Kere. (b) Pillow basalt at Maridihalli. (c) Elephant skin weathering of carbonate with interlayered chert close to Dodguni lime stone mines. (d) BIF with Jasper from roadside outcrop at 1 km SE of K.M. Kere in the Chitradurga basin.

6 Geochemistry and origin of greenstone volcanics and granitoids

6.1 ca. 3400–3150 Ma Sargur Group volcanics

The Sargur Group volcanics comprises dominantly of komatiite and komatiite basalts with minor basaltic to felsic pyroclastic flows. On the Al_2O_3–Fe_2O_3 + TiO_2–MgO ternary plot (Fig. 7a, c.f. Jayananda et al., 2023) and CaO–MgO–Al_2O_3 ternary plot (see supplementary figure S1) the Sargur Group volcanics plot on komatiite and one sample extending into komatiite basalts field. Both komatiites and komatiite basalts are characterized by moderate to high CaO/Al_2O_3 (1.06–1.59), low Al_2O_3/TiO_2 (7.7–23.6) and variable $(Gd/Yb)_N$ = 0.70–2.06 (Jayananda et al., 2016, 2023). The Sargur Group komatiites (Jayananda et al., 2016, 2023 and references therein) are characterized by low SiO_2 (38.91–46.86 wt%), Al_2O_3 (1.20–5.64 wt%) but conversely high MgO (42.40–25.12 wt%), Ni (1265–3694 ppm) whilst komatiite basalts contain slightly higher SiO_2 (48.50–49.10 wt%); lower MgO (12.9–15.6 wt%), Ni (265–1023 ppm). These komatiites and komatiite basalts contain sub-chondritic to moderate contents of total REE (0.38–36.28 ppm) and are characterized by moderately fractionated to flat REE patterns with variable $(Gd/Yb)_N$ = 0.70–2.06 (Jayananda et al., 2023; unpublished data). This coupled with their Nd isotopes ($\varepsilon Nd_{(T = 3350\ Ma)}$ versus Nb/Th Fig. 7b) incompatible element ratios (Nb/U versus Nb/Th; see supplementary figure S2) reveal origin of komatiites from heterogenous mantle reservoirs (depleted to primitive mantle). Their low SiO_2, high to very high MgO and high Ni–Cr coupled with low REE contents attributed to very high degree (about 50%) melting of deep mantle reservoirs. Their elemental characteristics like variable CaO/Al_2O_3 (1.06–1.59), Al_2O_3/TiO_2 $(Gd/Yb)_N$ = 0.70–2.06 with high Ni (1265–3694 ppm) and Cr (1627–4873 ppm) argue komatiite melt generation at different depths in deeper mantle (400–200 km) with retention of variable residual garnet or without garnet in residue. Incompatible elemental ratios like Nb/Y versus Zr/Y (Fig. 8a, c.f. Jayananda et al., 2023) and Zr/Nb versus Nb/Th (Figure not shown)

Fig. 5. (a) Massive ultramafic rock to the east of Shimoga basin at Santaveri–Lingadahalli road. (b) Mafic volcanicsin the road section (About 28 km from Shimoga in Narashimharajapura road). (c) Greywacke-argillite-chert with thin BIFs along western side of Shanthisagara reservoir. (d) Carbonaceous shale near Saulanga in Shikaripur–Shimoga road.

reveal their origin in hotspot environments and emplaced as oceanic plateaus whilst field evidence coupled with elemental data of few komatiites from Holenarsipur and Nuggihalli greenstone belt attributed their origin in oceanic arc setting or abducted section of oceanic lithosphere in spreading centre (Jayananda et al., 2023; Ma et al., 2024).

6.2 Dharwar Supergroup volcanics

6.2.1 Bababudan Group

The Bababudan Group represents intracontinental rift to passive margin succession (Chadwick et al., 1985) that preserve volcanic assemblages erupted on the >3150 Ma granitoid basement. Although Manikyamba et al. (2021) have documented wide range of ultramafic rocks from the NE part of the Bababudan basin, however, the documented ultramafic rocks in the NE part do not belong to Bababudan Group as our new field evidence reveal that ultramafic rocks overlying the stratigraphically youngest tuffs/BIFs which is also supplemented by isotopic age data. The Bababudan Group mafic volcanics display significant variation in elemental compositions (SiO_2 = 47.23–57.24 wt%; TiO_2 = 0.55–1.51 wt%; Al_2O_3 = 9.17–15.74 wt%; MgO = 4.54–10.85 wt%; CaO = 6.76–10.85 wt%; Na_2O = 0.73–3.46 wt%; 0.04–1.02 wt%). On Al_2O_3–Fe_2O_3 + TiO_2–MgO triangular plot (see Fig. 7a, c.f. Jayananda et al., 2023) they plot on high-Fe tholeiite field. The Bababudan Group volcanics are characterized by low to high abundances of incompatible elements including Sr (32.8–316.1 ppm), Ba (13–137.3 ppm), Th (0.39–7.23 ppm), U (0.04–1.66 ppm), Nb (1.20–9.90 ppm), Ta (0.02–0.75 ppm), Zr 10.4–146 ppm), Hf 0.48–3.53 ppm), Y (13.3–36.9 ppm) and REE (ΣREE = 30.08 to 158.41 ppm). The wide range of incompatible elements coupled with Nd isotopes [$\varepsilon Nd_{(T\ =\ 2920\ Ma)}$ = 2.1 to −1.32] reveal the origin of mafic volcanics from heterogeneous reservoirs ranging composition from depleted to primitive mantle (see supplementary figure S3) with variable crustal contamination of pre-existing crust which is consistent with Th/Nb versus TiO_2/Yb plot (Fig. 8b, after Pearce et al., 2021). Furthermore, moderately fraction-

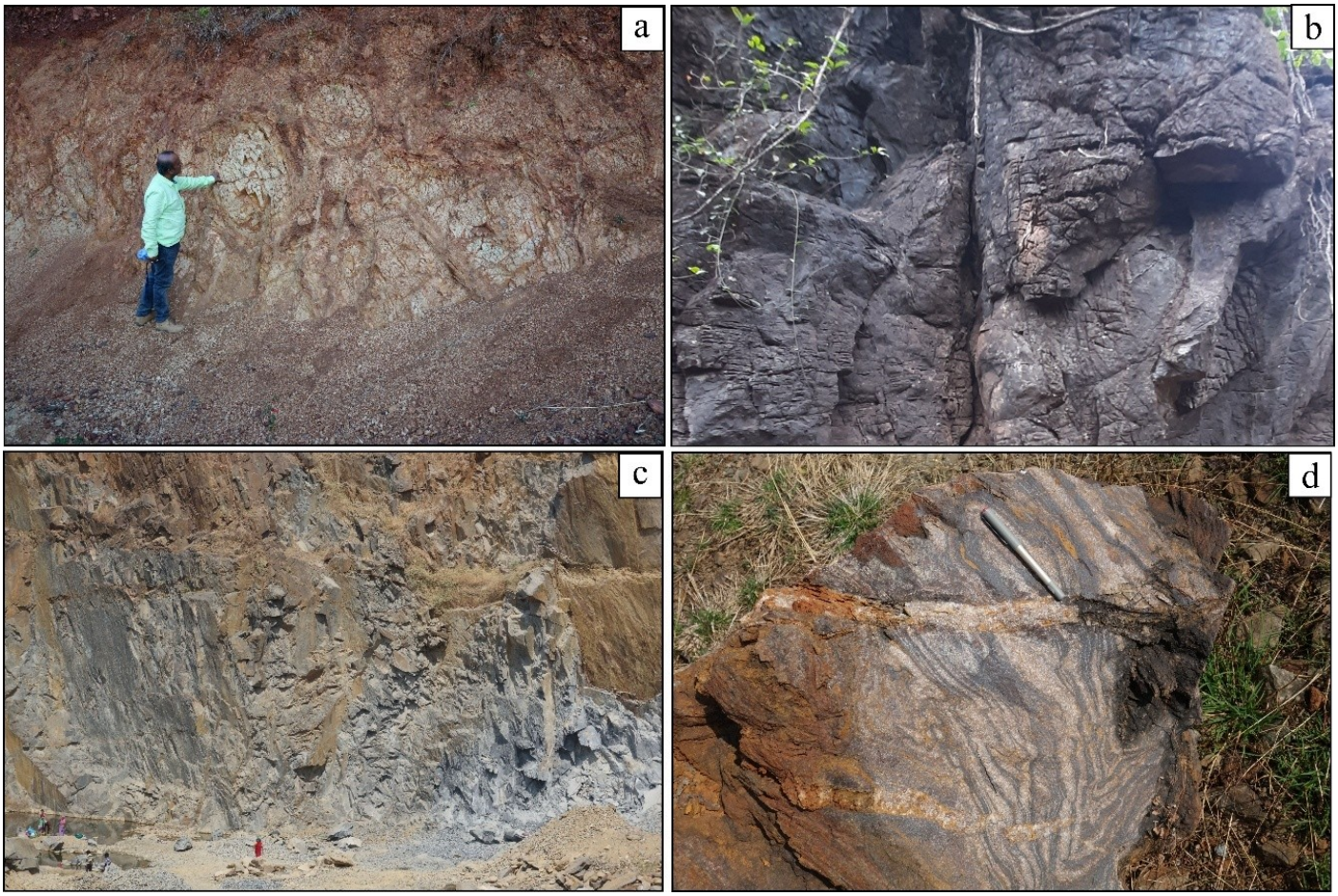

Fig. 6. (a) Weathered afic volcanics showing large pillows from southwestern part of the Dharwar basin in Shikaripura–Rattihalli road. (b) Massive arbonate rocks in the Dharwar basin close to Yana. (c) Greywacke in an active quarry 4 km ENE of Haveri. (d) Bouldary BIF outcrops of Dharwar basin to left side of the road the Bangalore–Pune National Highway 6 km before Ranibennur.

ated REE patterns with $(Gd/Yb)_N$ = 1.07–2.60 suggest that melts originated at different depths with or without retention of garnet in the source residue.

6.2.2 Chitradurga Group

The Chitradurga Group comprises bimodal volcanics including mafic and felsic rocks wherein mafic volcanics erupted ca. 2740 Ma (Kumar et al., 1996) whilst felsic volcanic flows erupted 2677 Ma (Jayananda et al., 2013). The mafic rocks are dominantly basaltic to basaltic andesite with few samples displaying basaltic komatiite composition (SiO_2 = 44.81–54.50 wt%; TiO_2 = 0.55–2.21 wt%; Al_2O_3 = 4.96–13.9 wt%; Fe_2O_3 = 8.01–13.90 wt%; MgO = 4.75–12.60 wt%; CaO = 4.29–14.9 wt%; Na_2O = 0.10–4.20 wt%; K_2O = 0.01–2.90). On the other hand, felsic pyroclastic flows to exhibit wide range of major element compositions [SiO_2 = 65.50–76.01 wt%; TiO_2 = 0.06–0.64 wt%; Al_2O_3 = 11.79–16.04 wt%; Fe_2O_3 = 0.18–5.96 wt%; MgO = 0.00–0.09 wt%; CaO = 0.17–3.10 wt%; Na_2O = 0.01–3.02 wt%; K_2O = 0.24–5.56 wt%]. On the Al_2O_3–Fe_2O_3 + TiO_2–MgO triangular plot (see Fig. 7a, c.f. Jayananda et al., 2023) Chitradurga Group mafic volcanics plot in high Fe-tholeiite to high-Mg tholeiite with few samples plot on komatiite basalt whilst felsic pyroclastic flows fall on dacite-rhyolite field. On the MgO versus FeO plot (see supplementary figure S4) Chitradurga volcanics plots on the fields of melts separated from source mantle before attaining equilibrium with mantle. These volcanics show wide range of trace element contents wherein mafic to intermediate volcanics display low to high Ba (11.93–307.5 ppm), Rb (0.97–54.85 ppm), Sr (24.88–333.9 ppm), Ni (13.6–316 ppm), Cr (23.0–450.6 ppm), Zr (37.25–134.36 ppm), Hf (0.97–3.63 ppm), Y (16.6–23.43 ppm), Nb (1.8–8.58 ppm), Ta (0.12–0.743 ppm), Th (16.6–23.43 ppm). Similarly, the felsic pyroclastic flows also exhibit large variation element contents wherein

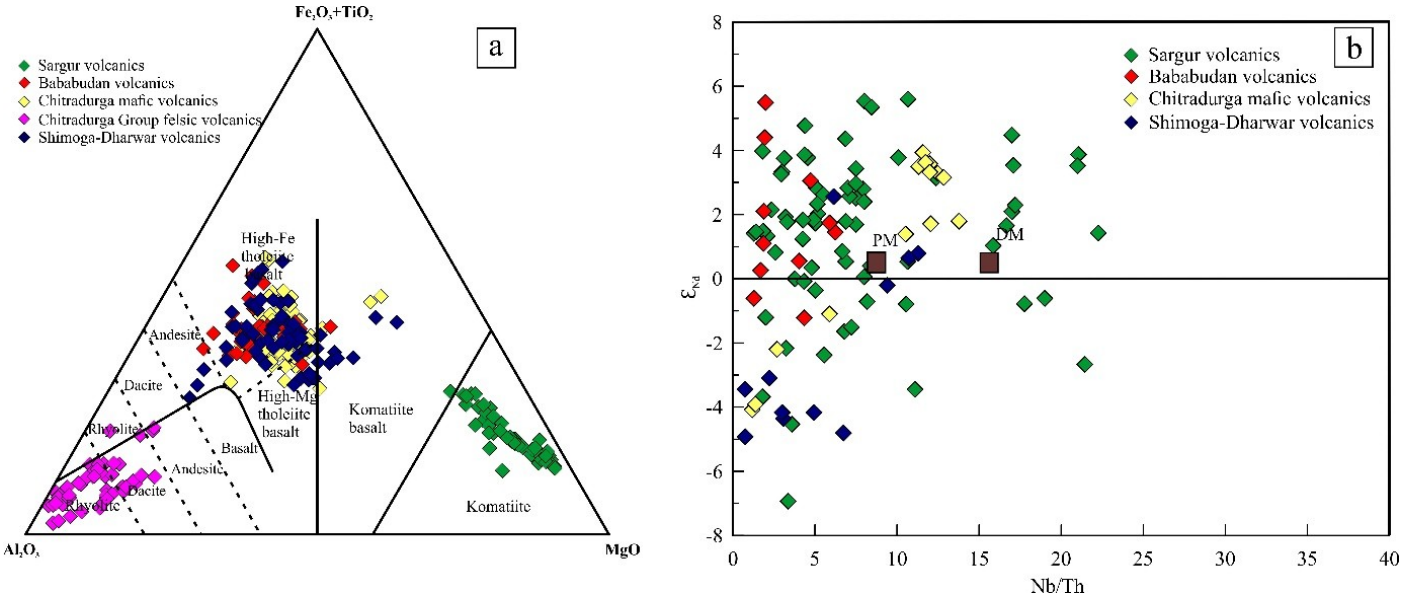

Fig. 7. (a) Al_2O_3–Fe_2O_3 + TiO_2–MgO (AFM) ternary plot (c.f. Jayananda et al., 2023) showing that ultramafic volcanic rocks of Sargur Group plot on komatiite field, whilst mafic volcanics of Dharwar Supergroup (Bababudan and Chitradurga Group) mainly fall on Fe-tholeiites with some samples extending into Mg-tholeiites field and Chitradurga Group felsic volcanics plot on rhyolite and dacite field. (b) $\varepsilon Nd_{(T\,=\,3350\ Ma)}$ versus Nb/Th of Sargur Group komatiites depict primitive (PM) to depleted mantle (DM) with some samples showing crustal contamination (Dharwar Supergroup (Bababudan and Chitradurga Group)) mafic volcanics fall on PM with several samples showing minor crustal influence.

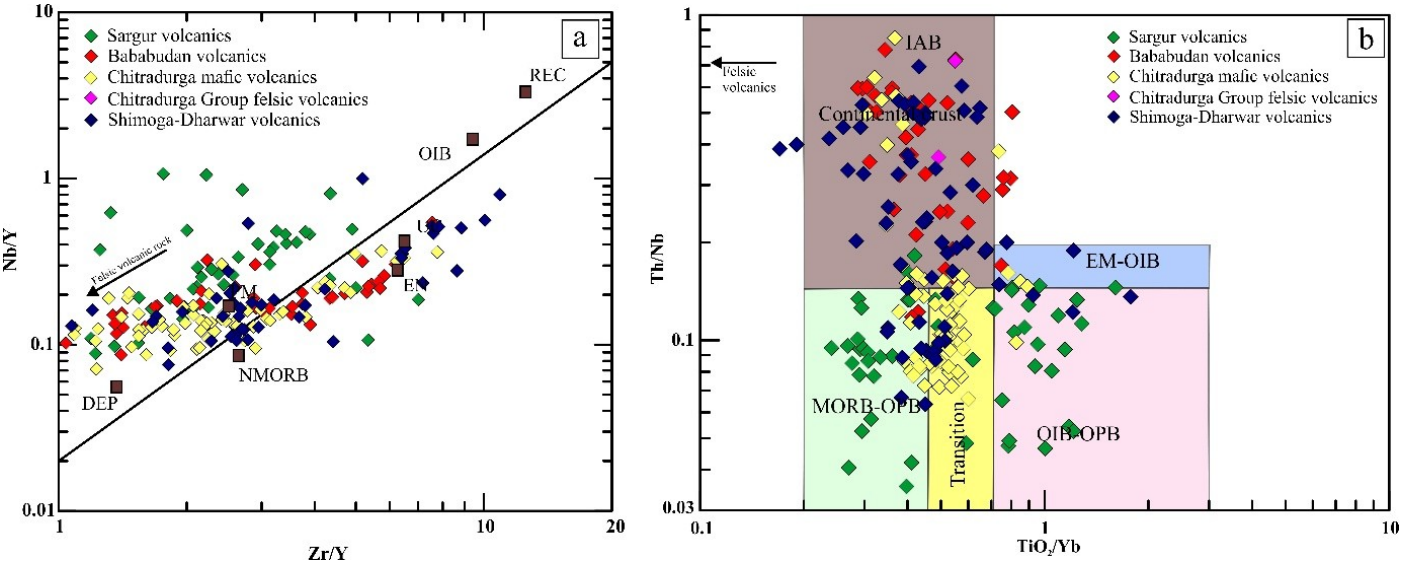

Fig. 8. (a) Nb/Y versus Zr/Y (c.f. Jayananda et al., 2023) indicating primitive mantle to MORB source reservoirs and few Dharwar Supergroup samples extending towards the upper crust contamination. (b) Th/Nb versus TiO_2/Yb (after Pearce et al., 2021) indicating the sources corresponding depleted mantle (MORB) to primitive mantle (OIB) for Sargur Group volcanics and arc mantle with continental crustal contamination for Dharwar Supergroup volcanics.

they show low to high Ba (12.00–475.0 ppm), Rb (21–239 ppm), Sr (7.0–186.9 ppm), Ni (0.20 to 92.7 ppm), Cr (1.9–169.7 ppm), Zr (23.58–707.7 ppm), Hf (0.75–20.1 ppm), Y (41.38–747.0 ppm), Nb (1.3–59.6 ppm), Ta (0.141–4.9 ppm), Th (0.80–27.00 ppm). Such wide range of trace element concentrations could be related to heterogeneity of their source reservoirs or involvement of pre-existing crust or contamination. The Chitradurga mafic volcanics show

large variations in total REE contents (26.22–149.26 ppm) and two distinct REE patterns wherein rocks with low total REE show flat patterns with $(Gd/Yb)_N$ ratios <1.0 whilst rocks with higher REE are moderately fractionated (see supplementary figure S5) with $(Gd/Yb)_N$ ratios 1.0–1.99. The REE patterns together with other incompatible element contents (Th, Ba, Sr, Zr, Y, Nb, Ta, Hf) reveal that Chitradurga volcanics originated from composite sources involving heterogenous mantle and pre-existing crust. Based on the incompatible element contents (Ba, Sr, Th, Zr, Hf, Y, Nb, Ta and total REE) two groups of mafic rocks being identified. Mafic rocks with high incompatible elements slightly lower MgO, Ni, Cr conversely higher SiO_2 and $(Gd/Yb)_N$ values (1.0–1.9) preclude their origin from depleted mantle as melts derived from depleted mantle impoverished in incompatible elements. Their low incompatible element contents coupled with flat REE patterns, and low $(Gd/Yb)_N$ depict high degree melting of shallow mantle. In contrast, the mafic volcanics with higher incompatible elements and fractionated REE patters [$(Gd/Yb)_N$ = >1.0 up to 1.9] imply their origin from lower degree melting of source reservoirs similar to primitive to enriched mantle at deeper level (see supplementary figure S5). Alternatively, such elemental characteristics could be related to contamination of pre-existing continental crust. Published Nd isotope data ($\varepsilon Nd_T = +2$ to -5; see supplementary figure S3; Kumar et al., 1996) suggesting heterogeneous mantle (depleted to primitive to enriched mantle) reservoirs and variable crustal contamination. This is in consistent with incompatible element ratios (Nb/Th versus Nb/U; see supplementary figure S2) and Nb/Y versus Zr/Y (see Fig. 8a, c.f. Jayananda et al., 2023). Pressure sensitive incompatible elements and their ratios like Sm/Yb versus Sm (Fig. 8(c), c.f. Aldanmaz et al., 2000) are used to evaluate the sources and depth of melting wherein Chitradurga mafic volcanics plot along spinel-lherzolite, spinel-garnet lherzolite suggesting origin of mafic magmas at different depths in the shallower mantle without or with minor garnet in residue.

The high SiO_2, alkalis, high incompatible trace elements including REE (203.28–747.38 ppm) coupled with MgO, Ni and Cr of felsic pyroclastic flows preclude their derivation by direct melting of mantle. Their time relationships with mafic volcanics, high total REE coupled fractionated patterns with [$(La/Yb)_N$ = 2.06 to 26.69] ratios and strong negative Eu anomalies (Eu/Eu* = 0.11 to 0.78) suggest involvement of newly formed arc crust and combination of arc crust and pre-existing continental crust (TTGs?) in their genesis. This is in agreement with Nd isotope data ($\varepsilon Nd_{(T\,=\,2700\,Ma)} = +1.5$ to -1) suggesting derivation of felsic pyroclastic flows by melting source involving newly formed arc crust and pre-existing crust (see supplementary figure S3).

To summarize, elemental and Nd isotope data suggest Chitradurga mafic volcanics originated from heterogenous source reservoirs including depleted to primitive mantle with minor crustal contamination whilst felsic volcanics derived from arc crust melting and minor involvement of pre-existing gneisses in arc settings.

6.2.3 Shimoga–Dharwar basin volcanics

Shimoga–Dharwar basin corresponds to upper part of Chitradurga Group where Sm–Nd whole rock isochron of mafic volcanics define ca. 2638 ± 66 Ma (Giri et al., 2019) whilst U–Pb zircon age of felsic volcanics indicate 2614 ± 1.9 Ma to 2605 ± 5 Ma (Nutman et al., 1996; Corfu and Hegde, 2020). This greenstone belt preserves mafic to felsic volcanic sequences with few ultramafic rocks found as tectonically transported fragments. The volcanics exhibit wide range of major element compositions including SiO_2 (42.06–60.71 wt%), MgO (3.7–15.27 wt%), Fe_2O_3 (7.24–18.01 wt%), CaO (2.72–19.61 wt%) low K_2O (0.07–2.3 wt%). On Harker's binary plots these volcanics show weak to moderate negative correlation of SiO_2, Fe_2O_3 and CaO against MgO indicate minor fractionation of olivine, pyroxene and plagioclase whilst ultramafic rocks show restricted range of major element contents and do not display differentiation trend (figure not given). On Al_2O_3–Fe_2O_3 + TiO_2–MgO triangular plot (see Fig. 7a, c.f. Jayananda et al., 2023) Shimoga–Dharwar volcanics plot in high-Fe tholeiite extending into high-Mg tholeiite and andesite field. The Shimoga volcanics exhibit low high total REE contents (19.08 to 246.05 ppm) and display poorly to moderately fractionated REE patterns [$(Gd/Yb)_N$ = 0.85 to 2.41] without any Eu anomalies. On the other hand, Dharwar volcanics contain low to moderate total REE (27.5 to 169.87 ppm) with poor to moderately fractionated (see supplementary figure S5) REE patterns [$(Gd/Yb)_N$ = 1.07 to 2.05]. Their wide range of incompatible element contents coupled with REE patterns of Shimoga–Dharwar volcanics reveal their derivation from heterogenous source reservoirs. This is consistent with incompatible element ratios of Nb/Th versus Nb/U plot (see supplementary figure S2) and Nb/Y versus Zr/Y (c.f. Jayananda et al., 2023) wherein they plot in depleted to primitive mantle with minor crustal contamination (see Fig. 8a). On the Th/Yb versus Nb/Yb plot (see supplementary figure S6) Shimoga–Dharwar volcanics follow the arc-like enrichment trend. Sm/Yb versus Sm plot (see Fig. 8(c), c.f. Aldanmaz et al., 2000) used to characterize magma origin in mantle at different depths where in the Shimoga–Dharwar volcanics follow trend corresponding to 15–30% melting spinel lherzolite to garnet lherzolite mantle. Zr/Nb versus Nb/Th plot (figure not shown) used to characterize the tectonic context of magma genesis wherein the Shimoga–Dharwar basin volcanics mainly plot in arc setting with few samples extending into OIB and crustal contamination.

The ultramafic rocks in the Shimoga basin show very low incompatible element contents with sub-chondritic REE

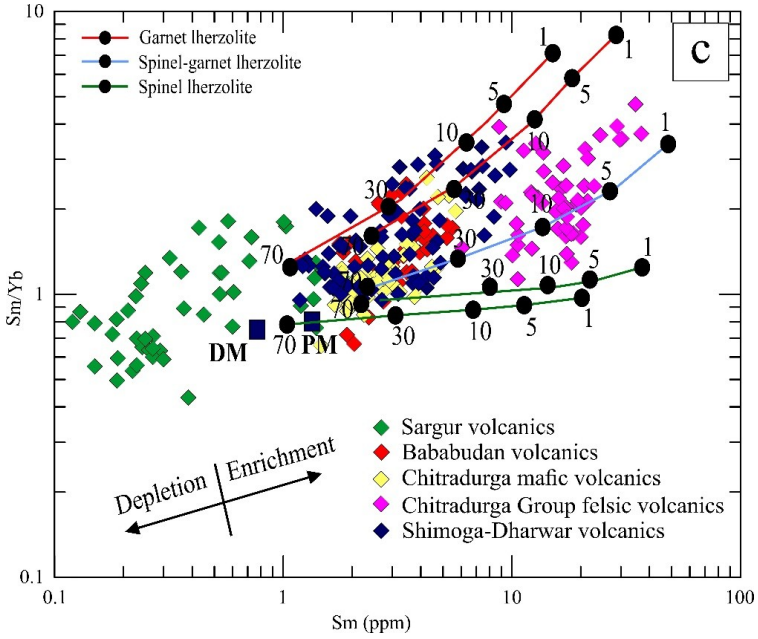

Fig. 8(c). Sm/Yb versus Sm (c.f. Aldanmaz et al., 2000) indicating the depletion and enrichment with respect of spinel-lherzolite, spinel-garnet lherzolite and garnet-lherzolite for the Sargur and Dharwar Supergroup rocks. DM = Depleted Mantle; PM = Primitive Mantle.

contents (<5 ppm) and show flat patterns with $(Gd/Yb)_N$ < 1.0 suggesting their derivation from highly depleted mantle similar to N-MORB. Indeed, these rocks found as fragments in association with greywacke-argillite appears to be tectonically transported in arc environments.

In summary, Shimoga–Dharwar basin volcanics originated from heterogenous mantle at different depths with minor crustal contamination whilst ultramafic rocks from Shimoga basin are derived from depleted sources similar to N-MORB.

7 Origin of Archean granitoids

7.1 ca. 3400–3200 Ma TTG-type granitoids

Several integrated studies focused on the TTG-type gneisses in the western Dharwar craton (Jayananda et al., 2023 and references therein). Archean granitoids of TTG affinity show a wide range of compositions with SiO_2 ranging from 60.58–79.70 wt% (Jayananda et al., 2023; and references therein). On the Ab–An–Or triangular plot (see supplementary figure S7) most of the gneisses plot in trondhjemite and tonalite with few samples extending into the granodiorite field. On the Q–Ab–Or diagram (see supplementary figure S8) and K–Na–Ca plot (see supplementary figure S9) the gneisses follow trondhjemite differentiation trend typical of Archean TTGs. Based on Al_2O_3 contents two groups of TTGs are documented in the WDC i.e. older (>3350 Ma) low-Al_2O_3 (<14.0 wt%) whilst younger (<3350 Ma) high-Al_2O_3 gneisses. These gneisses show metaluminous to peraluminous character and display moderate to strong negative correlations of major oxides (TiO_2, Al_2O_3, Fe_2O_3, MgO and CaO) against SiO_2 (Jayananda et al., 2018; figure not given) indicating fractionation of hornblende/pyroxene, plagioclase, Fe–Ti oxides or their retention in source residue. On the Al_2O_3/FeO + MgO–3CaO–5K_2O/Na_2O triangular plot (Fig. 9a, c.f. Jayananda et al., 2023) about 70% of the gneisses fall on the low-K mafic source with about 25% of samples tonalitic samples and about 5% samples extend into high-K mafic source suggesting their derivation from low-K mafic rocks with significant remelting of pre-existing gneisses. The low-Al_2O_3 gneisses contain higher MgO despite higher SiO_2 contents and show low to high total REE (36–316 ppm) and poorly fractionated REE patterns [$(La/Yb)_N$ = 1.78–6.97] with negative Eu anomalies (0.58–0.72) suggest their derivation from low-pressure melting of depleted mafic source rocks and pre-existing gneisses within plagioclase stability field and without garnet in source residue (Jayananda et al., 2015, 2023). In contrast highly fractionated REE patters of high-Al_2O_3 gneisses with [$(La/Yb)_N$ = 14.13–33.74] reveal their origin by moderate to high pressure melting of mafic source rocks with variable hornblende, plagioclase, garnet and Fe–Ti oxides in source residue (Jayananda et al., 2015). These observations of origin of gneisses from low-K to high-K mafic rocks including involvement of pre-existing crust at different depths with or without residual garnet is also in consistent with Sr/Y versus K_2O/Na_2O + CaO plot (Fig. 9b, c.f. Jayananda et al., 2023), Sr/Y versus Y

(Fig. 10a, c.f. Jayananda et al., 2023) and $(La/Yb)_N$ versus $(Yb)_N$ plot (Fig. 10b, c.f. Jayananda et al., 2023). Whole rock Nd isotope ($\varepsilon Nd_{(T)}$ = +3.5 to −2.5 (see supplementary figure S3); $\varepsilon Hf_{(T)}$ = +5 to −2.2) of the gneisses reveal their origin from juvenile mafic rocks and pre-existing crustal rocks. The tectonic context of TTGs origin is topic of much discussion. Various models have been proposed including melting of arc crust at different depths (Jayananda et al., 2015), melting of the base of oceanic plateau and oceanic arc crust (Jayananda et al., 2023) explain the elemental characteristics of the TTGs. Melting of subducting oceanic crust produced at the spreading centre depleted and cannot explain the high incompatible element contents of the TTGs. Alternatively, two stage melting (Polat, 2012) proposed to explain the origin of TTGs which include melting of oceanic crust in subduction zone to build an oceanic arc crust and remelting of arc crust at different depths explain the elemental characteristics of TTGs. Furthermore, some older (>3350 Ma) TTGs (Jayananda et al., 2015) show unusual elemental characteristics like high MgO (>0.60 upto 1.6 wt%) high SiO_2 (>73.0 wt%) with poorly fractionated REE and strong negative Eu anomalies which cannot be explained by melting of arc crust in subduction zone settings. Alternatively, low pressure (<10 kbar) melting of crust at base of the oceanic plateau can be considered. Melting of such oceanic plateau crust at shallower depth can explain the observed elemental characteristics of the TTGs (Jayananda et al., 2023).

To summarize, the TTG-type gneisses in the WDC originated by low to high pressure melting of juvenile mafic source and minor involvement of pre-existing gneisses with hornblende, plagioclase, Fe–Ti oxides with or without garnet in source residue.

7.2 ca. 3150 Ma Chikmagalur granite

The ca. 3150 Ma Chikmagalur granite is a funnel shaped intrusion into the old Archean basement (TTG and Sargur Group). This granite contain quartz, plagioclase, K-feldspar, biotite with occasional hornblende coupled with accessory zircon, apatite, titanite and opaque phases. U–Pb zircon ages indicate 3153 ± 4 Ma and 3154 ± 6 Ma whilst the surrounding TTG gneisses ca. 3350–3280 Ma (Jayananda et al., 2015). This pluton shows a restricted range of major element composition with SiO_2 (72.97–74.76 wt%), lower Al_2O_3(13.04–14.05 wt%), Fe_2O_3 (2.06–1.45 wt%), CaO (1.65–1.44 wt%), Na_2O (4.48–4.25 wt%) and K_2O (3.49–2.90 wt%). It shows a transitional character from TTGs to potassic granite composition and follows calc-alkaline differentiation trend (Jayananda et al., 2015). They contain moderate incompatible elements (Rb = 102–73 ppm; Sr = 201–114 ppm; Ba = 392–368 ppm) including REE (178–101 ppm). The REE patterns are moderate to highly fractionated with $[(La/Yb)_N$ = 10.70–32.62] with feeble negative Eu anomalies. Their relatively low to moderate Rb, Sr, Ba, REE contents together with mild negative Eu anomalies coupled with Nd isotope data ($\varepsilon Nd_{(T)}$ = −0.9 to −1.7) suggest their origin by lower crustal melting of newly formed TTGs with lesser crustal residence time. The tectonic context of magma generation and emplacement is not clear, however, recent field and detrital zircon age record of associated Karthikere conglomerate attributed to continental collision during ca. 3150 Ma (Mallens et al., 2023).

7.3 ca. 3000–2950 Ma and ca. 2620 Ma potassic plutons

Both ca. 3000–2950 Ma and ca. 2620 Ma plutons display similar petrographic characteristics containing quartz, K-feldspar, biotite, hornblende and primary epidote in the mineral assemblage. These plutons rarely contain fragments of large kyanite bearing pelites along their margins. The presence of primary epidote and euhedral quartz imply rapid emplacement. They exhibit significant variation in SiO_2 (63.69–76.83 wt%), Al_2O_3 (12.4–15.95 wt%), ferromagnesian elements (Fe_2O_3 = 0.51 to 5.85 wt%), MgO (0.02 to 2.63 wt%) and high-potassium (K_2O = 3.08 to 5.68 wt%). On Ab–An–Or triangular plot these rocks plot on granodiorite to granite fields with few samples extending to quartz-monzonites (see supplementary figure S7) whilst display calc-alkaline differentiation trends on the Q–Ab–Or (see supplementary figure S8) and K–Na–Ca triangular diagrams (see supplementary figure S9). On Harker's binary plots both groups of potassic granites show differentiation trends where moderate to strong negative correlation of TiO_2, Al_2O_3, Fe_2O_3, MgO and CaO against SiO_2 (Figure not given; Jayananda et al., 2019) indicate hornblende, plagioclase, Fe–Ti oxide control as fractionating phases or residual phases. These potassic plutons are characterized by variable but generally high content of incompatible elements (Ba, Rb, Sr, Y and REE). The REE (71–826 ppm) are characterized by poor to highly fractionated REE patterns $[(La/Yb)_N$ = 2.74–57.10] with very strong negative Eu anomalies [(Eu/Eu* = 0.09–0.71) see supplementary figure S10] suggesting their origin at shallower depths within plagioclase stability field wherein plagioclase, hornblende or pyroxene, Fe–Ti oxides in residue. On the Al_2O_3/FeO + MgO–3CaO–5K_2O/Na_2O triangular plot (see Fig. 9a, c.f. Jayananda et al., 2023) most samples plot on high-K mafic to pre-existing tonalite source with few samples extending to metasedimentary source which is conformity with numerous mafic, TTGs and rare metasedimentary enclaves in the potassic granites (Jayananda et al., 2019). Whole rock Nd isotope data ($\varepsilon Nd_{(T)}$ = +2.0 to −7.9; see supplementary figure S3) indicate their derivation mainly by reworking of ancient crust with involvement of minor LREE depleted juvenile source (Jayananda et al., 2019).

Pressure sensitive elemental ratios of potassic granites projected on the plot like Sr/Y versus K_2O/Na_2O + CaO (c.f. Jayananda et al., 2023) indicate their origin by low to medium pressure melting of enriched mafic source

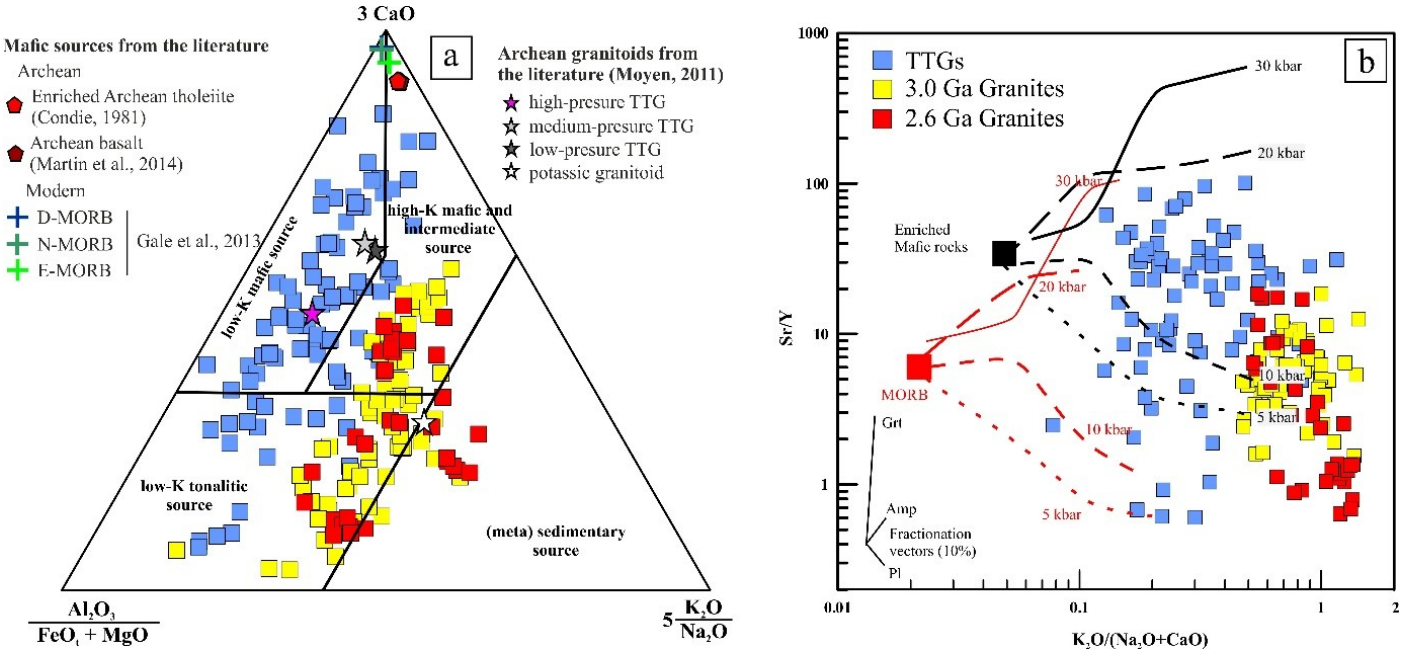

Fig. 9. (a) $Al_2O_3/(FeO_t + MgO)$–3*CaO–5*(K_2O/Na_2O) diagram (c.f. Jayananda et al., 2023) showing the low to high-K mafic sources along with input from pre-existing tonalite for the TTGs and high-K mafic to intermediate sources with few extending into meta-sedimentary input for the 3.0 Ga, 2.6 Ga potassic granites. (b) $K_2O/(Na_2O + CaO)$ versus Sr/Y plot (c.f. Jayananda et al., 2023) representing the melts originate from depleted and enriched mafic rocks at different pressures; broken lines correspond to melting models derived from experimental database, at different pressures and for two sources, depleted and more enriched mafic rock.

(see Fig. 9b). This is in consistent with other pressure sensitive elemental ratios of Sr/Y versus Y plot (see Fig. 10a, c.f. Jayananda et al., 2023) and $(La/Yb)_N$ versus $(Yb)_N$ plot (see Fig. 10b) where potassic granites plot on low to moderate pressure melting without any significant garnet in source residue. The tectonic context of the magma generation and emplacement of potassic plutons is not clearly known. The emplacement of potassic granite in Archean cratons globally considered to coincide with stabilization of continental crust. These potassic granite show characteristics of A-type granites on Nb/Y versus Ta + Yb plot (see supplementary figure S11) where they plot on slab failure to A-type granite. Consequently, these potassic granites probably emplaced during collision of micro-blocks or slab break off associated with arcs collision.

In summary, potassic granites originated by low to moderate pressure melting of composite sources involving dominant pre-existing crust with minor depleted juvenile input in collisional settings.

8 Archean sedimentary record and surface environments

8.1 Provenance and depositional environments

The preserved Archean greenstone sedimentary sequences in the stratigraphic record of Sargur Group and Dharwar Supergroup preserve a record of evolving redox conditions ocean-atmospheric system, shift from anoxic to oxygenated environments and biologic activity from ca. 3400–2600 Ma. These assemblages are key to our understanding of redox conditions of surface environments, microbial recycling and oxygenation of oceans. The Sargur Group sediments comprise quartzite/conglomerate, pelites, carbonates and BIFs indicating their deposition mainly in stable shallow shelf environments. Among the Dharwar Supergroup sedimentary sequences, the Bababudan Group basins contain oligomictic conglomerates, quartzite with cross-bedding, phyllites, and thick BIFs sequence. Such assemblages indicate their deposition in stable shallow environments to progressively deeper environments. The conglomerates with rounded clasts were interpreted as involving large degree shallow shelf environments (Srinivasan and Ojakangas, 1986) or fluvial environments (Chadwick et al., 1985). The quartzites layers with cross-bedding associated with basaltic flows likely deposited in stable shallow environments during quite periods whilst phyllites and BIFs deposited progressively more deeper environments. The matured detritus includes clean rounded pebbles and sand to silt sized materials sourced from much older stable continental landmass and involved in long transport. In contrast the younger basins (Chitradurga, Dharwar–Shimoga) com-

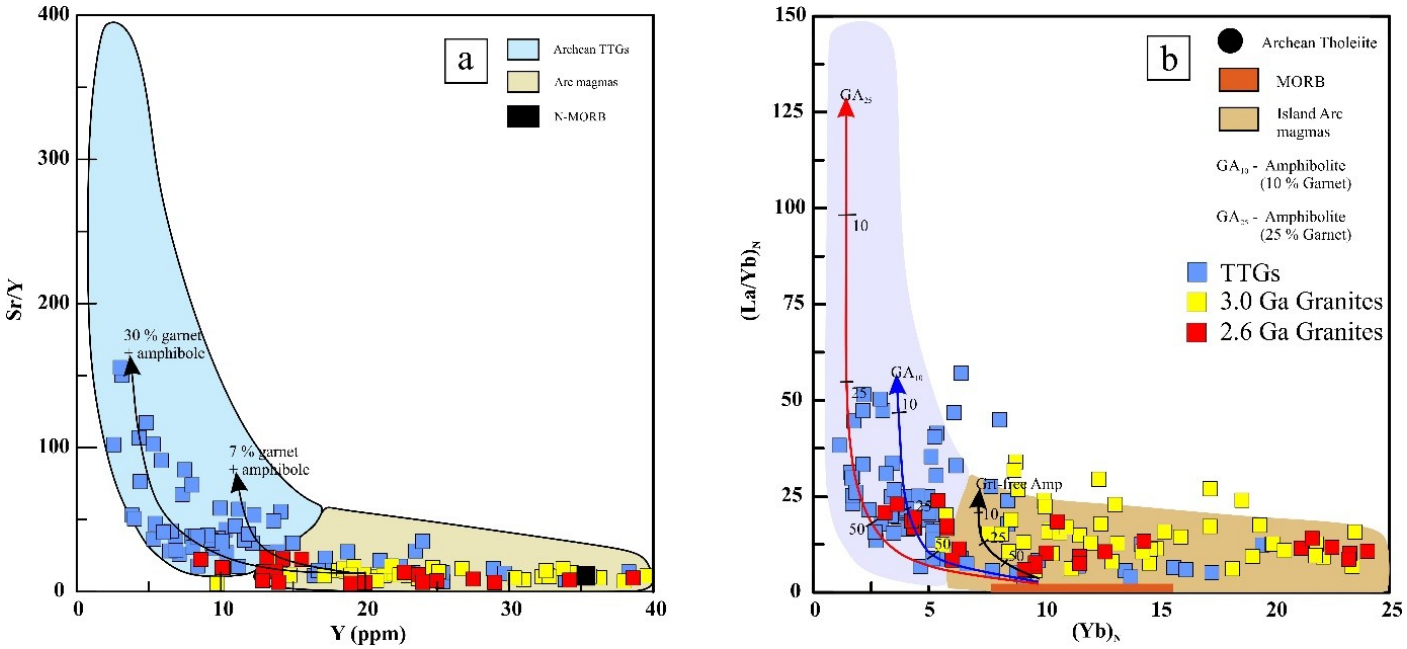

Fig. 10. (a) Sr/Y versus Y (c.f. Jayananda et al., 2023) showing sources of TTGs, potassic granites and the role of residual garnet. Arrows indicate batch melting of mafic source with 7–30% garnet-amphibole in source residue. (b) $(La/Yb)_N$ versus Yb plot (c.f. Jayananda et al., 2023) showing TTGs derived from distinct mafic sources with or without residual garnet. Arrows in field indicate batch of melting of mafic source at deeper levels transforming into garnet bearing amphibolites residue with 7–30% garnet in residue. Abbreviations used: Gt = garnet; Amp = amphibole.

prise polymict conglomerate of glacimarine origin (Ojakangas et al., 2014), greywacke-argillite-carbonaceous shales-BIFs points to deposition of detritus in unstable shallow to deeper environments by rapid erosion of adjacent basement and newly formed magmatic arcs causing dumping into the basin.

Focused research on sedimentology of the Sargur Group and Bababudan Group sedimentary sequences is rather poor except the discussion on depositional environments of conglomerate and quartzite (Chadwick et al., 1985; Srinivasan and Ojakangas, 1986). The basal conglomerate with interbedded quartzite successions interpreted as shallow tidal marine environments (Chadwick et al., 1985) whilst Srinivasan and Ojakangas (1986) interpreted depositional environment as a dominant braided fluvial plain on a peneplaned granitic crust.

The published data of sedimentary rocks from Chitradurga and Shimoga–Dharwar basin mostly falls in the field of shales, quartz-arenite, lith-arenite and greywacke in the Log (SiO_2/Al_2O_3) vs Log (Fe_2O_3/K_2O) and Log (Na_2O/K_2O) diagrams (see supplementary figure S12 and S13). The geochemical characteristics of shale, carbonaceous shale/phyllite (Sindhuja et al., 2022) stromatolitic dolomite (Khelen et al., 2019) carbonates from Chitradurga and Shimoga (Govind et al., 2021) and Qtz–Fe–Mn arenites, argillites (Harshitha et al., 2024) are well presented. Similarly, the greywackes geochemical characteristics from Shimoga–Dharwar basin are presented by Ugarkar et al. (2017). The chemical index of alteration (CIA) is used to access the weathering condition and metasomatism which affects significantly the geochemical characteristics of the clastic sediments (Fedo et al., 1995) and CIA values above 80 have considered to be the effect of intense chemical weathering and metasomatism, on the other hand CIA values less than 50 have insignificant effect on weathering. The western Dharwar sedimentary rocks show low to moderate weathering, majority of the samples falls less than ($\leq$80) in the chemical index of alteration (CIA) versus Al/Na bivariant diagram (see supplementary figure S14). Further, Fedo et al. (1995) have evaluated the mineralogical changes during the diagenesis, K-addition which reflects the weathering progress and K-metasomatism. The majority of the sedimentary samples in the CN–Al–K ternary diagram (see supplementary figure S15) plots towards the Al_2O_3 apex and it reveals the possible source that the protolith contain more alumina and hence roles out the K-addition and metasomatism. This is further substantiated by the elemental ratio diagrams of Zr/Sc versus Th/Sc (Fig. 11a, c.f. Harshitha et al., 2024); La/Sc versus Co/Th (Fig. 11b, c.f. Sindhuja et al., 2022) which indicates mafic to intermediate source provenance with very minor sediment recycling.

The Post Archean Australian Shale (PAAS) normalized REE+Y of shale and greywackes show chondritic

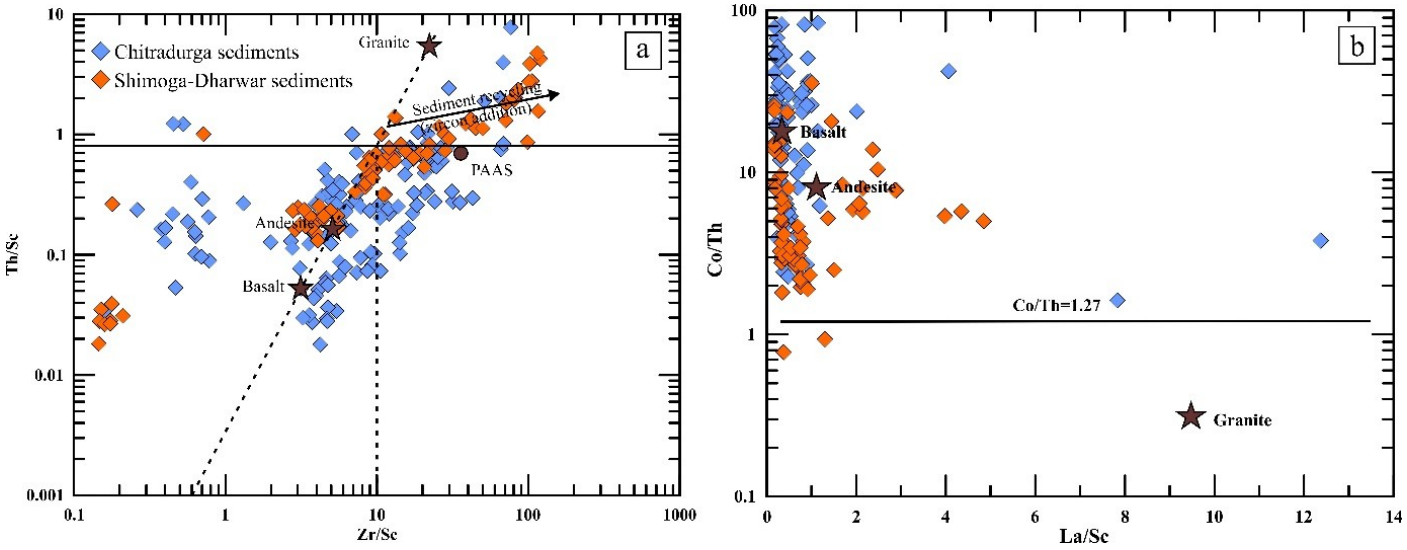

Fig. 11. (a) Zr/Sc versus Th/Sc binary plot (c.f. Harshitha et al., 2024) showing the dominant mafic to intermediate source provenance for the Chitradurga, Shimoga–Dharwar sediments. (b) La/Sc versus Co/Th (c.f. Sindhuja et al., 2022) indicating the dominant mafic to intermediate source provenance for the Chitradurga, Shimoga–Dharwar sediments.

pattern while carbonaceous shale/phyllite, carbonates, stromatolitic dolomite, arenites show sub-chondritic REE+Y patterns which in turn suggesting that their provenance originated from depleted mantle (see supplementary figure S16, figures given only for carbonate rocks).

Redox conditions of Archean surface environments in the Dharwar craton are poorly known except few studies attempted in recent years (Hashizume et al., 2016; Mishima et al., 2017; Khelen et al., 2020; Govind et al., 2021; Harshitha et al., 2024; Mukherjee et al., 2025). The Dharwar craton preserve sedimentary sequences in the entire stratigraphic record from older Sargur Group and younger Dharwar Supergroup. Recently, combined mineralogic and redox sensitive elemental on the BIFs of the ca. 3300–2600 Ma BIFs from Sargur Group and Dharwar Supergroup reveal dominantly anoxic environments during deposition of older sedimentary assemblages in Sargur Group whilst fluctuating redox conditions during development of younger Dharwar Supergroup with minimum oxygen on the ocean surface which linked to deposition of BIFs with alternate bands of iron oxides and chert (Hashizume et al., 2016; Mukherjee et al., 2025). The clean pebbles with matrix in oligomict conglomerates containing sulphides and occasional uraninite reflect dominant anoxic environments. Furthermore, the arenite /quartzite layers associated with mafic volcanic flows and argillite (now phyllite) reveal shallow to deeper environments without free oxygen on ocean surface. On the other hand, a paradigm shift in the surface environments with the appearance of BIFs in the higher stratigraphic levels related periodic fluctuations oxygen appearance on ocean surface probably linked to microbial activity (Hashizume et al., 2016). The younger Chitradurga Group comprises two major sedimentary basins including ca. 2700–2640 Ma Chitradurga and ca. 2638–2600 Ma Shimoga–Dharwar basin. The Chitradurga basin preserve siliciclastic including polymictic conglomerate, stromatolitic carbonates, thick greywacke-argillite-carbonaceous shale and BIFs (Khelen et al., 2020; Harshitha et al., 2024) reflecting shallow to deeper environments from WSW towards ENE. The presence of sulphides in the sedimentary sequences including siliciclastic, greywacke-argillite-carbonaceous shales and some BIFs suggest dominant anoxic environments which is in conformity with results of mass independent fractionation of sulphur isotopes (Mishima et al., 2017). On the other hand, redox sensitive element ratios of BIFs indicate periodic fluctuations in oxygen appearance on the ocean surface (Mukherjee et al., 2025). The presence of carbonate beds with layers of cherts and stromatolite with algal mats along the western margin of the Chitradurga basin points to shallower environments with fluctuation in oxygen activity on ocean surface. Recent elemental data from Vanivilas Formation of Chitradurga basin such as depleted LREE with slightly enriched HREE coupled with higher Y/Ho ratios and varying Ce anomalies (few samples with negative Ce anomalies); Fig. 12a, (Pr/Pr* versus Ce/Ce* c.f. Govind et al., 2021) as attributed to marine origin with local shallow oxygenated Neoarchean Ocean (Govind et al., 2021). It further strengthens by the Nd versus Ce anomaly binary plot wherein majority of the sediments in anoxic condition with few extending to oxic condition through transition (Fig. 12b, c.f. Mukherjee et al., 2025). Further, Carbon (δ^{13}C mean = −0.27‰) correlated and oxygen (δ^{18}O mean = −10.78‰) isotope ratios of the carbonates attributed to

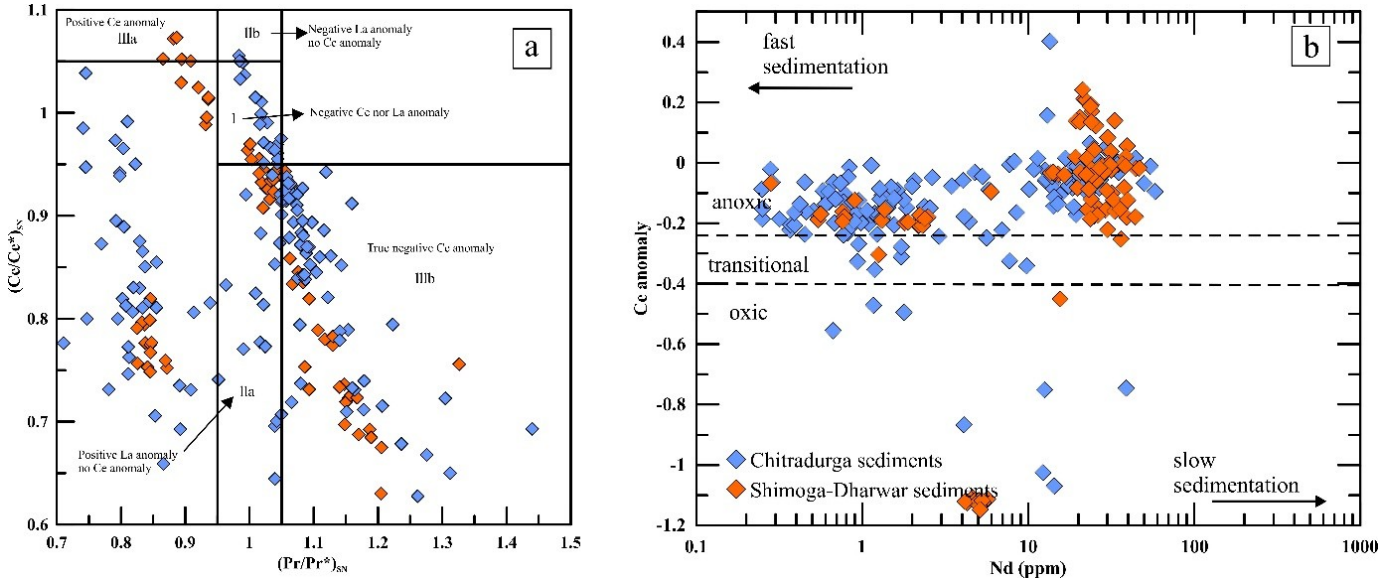

Fig. 12. (a) $(Pr/Pr^*)_{SN}$ versus (Ce/Ce*) Ce anomaly plot (Govind et al., 2021). Field I: samples with neither Ce anomaly nor La anomaly. Field II: samples with positive La anomaly and no Ce anomaly. Field III: samples with negative Ce anomaly (only samples with $Pr/Pr^* > 1.1$ are considered to have a negative Ce anomaly). (b) Ce anomaly versus Nd (c.f. Mukherjee et al., 2025) contents showing the transition from the anoxic to oxic environmental conditions.

later interaction with diagenetic or meteoritic fluids. Nd–Sr isotopic compositions of these carbonates reveal input from continental sources and marine hydrothermal plumbing system from depleted mantle (Govind et al., 2021) whilst Pb-isotope compositions attributed to sources from less evolved sources probably from different lithospheric plates (Russell et al., 1996).

The Shimoga–Dharwar basin preserve largest Neoarchean sedimentary record with shallower continental shelf environment to the WSW which progressively become deeper to the ENE. No detailed biomarker study involving redox sensitive elements and isotopes initiated to evaluate redox conditions of Neoarchean Shimoga–Dharwar basin. Recent stable isotope data such as $\delta^{13}C$ ranging -0.30 to 1.29‰ VPDB combined with negative $\delta^{18}O$ values of -20.95‰ to -7.72‰ VPDB indicate fluctuating oxic to anoxic acidic to alkaline environments during the formation of stromatolites with varying sea water temperatures range from 25 °C to 75 °C (Khelen et al., 2020). These authors attribute the deposition of carbonates in shallow shelf environments ranging from supra to sub-tidal conditions with a contribution mantle sourced hydrothermal plumbing.

9 Discussion

9.1 Archean thermal records and their spatial link to magmatism and crustal reworking

The Archean Dharwar craton affected by several thermal events which are spatially linked to crust accretion, reworking of pre-existing, emplacement of granite plutons and development of cratonal architecture (Jayananda et al., 2013, 2020, 2023). The western Dharwar craton witnessed three major thermal events during ca. 3150 Ma, ca. 3000–2950 Ma, and ca. 2500 Ma (Jayananda et al., 2013; Kaempf et al., 2025). Discordant U–Pb zircon ages, U–Pb titanite and U–Pb monazite ages of gneisses and metapelites in the Holenarsipur region document earliest thermal record of ca. 3150 Ma (Jayananda et al., 2013). This thermal event immediately preceded by the intrusion of diapiric trondhjemite which spatially linked to assembly of different tectonic units including oceanic plateau, oceanic arc and oceanic ridge and a micro-continent through horizontal motion development of dome-keel architecture (Jayananda et al., 2023). *in-situ* Lu–Hf dating of garnet indicate ca. 3.0–2.95 Ma thermal event in the Kalyadi region (Kaempf et al., 2025) which spatially probably linked to the collision of volcanic arc/volcanic plateau with micro-continent followed by slab break off driving the mantle upwelling causing lower crustal melting and emplacement of ca. 3000–2950 potassic plutons (present study; Jayananda et al., 2019). The ca. 2500 Ma thermal event affected the whole Archean crust of the Dharwar craton (Jayananda et al., 2013; Dasgupta et al., 2019; Kaempf et al., 2025). Recent *in-situ* Lu–Hf dating garnet from Holenarsipur region yielded ca. 2513 Ma (Kaempf et al., 2025) which in agreement with earlier Sm–Nd garnet-whole rock isochrons and U–Pb monazite ages (Jayananda et al., 2013). To summarize, Archean crust in the WDC involved in three major events which spatially associated with

magmatic accretion, reworking of pre-existing crust and amalgamation of different tectonic units marking episodes of cratonization of Archean continental crust.

9.2 Major episodes of crust formation and rates of continental growth

The widespread TTG-type gneisses and associated volcanic sequences corresponds to preserved Archean continental crust in the WDC formed during successive stages of juvenile crust accretion and remelting of pre-existing crust with different crustal residence time. U–Pb zircon dating of TTG-type granitoids in the cratonic core (Hassan–Gorur–Holenarsipur region) adjoining areas reveal three major episodes of felsic continental crust formation during ca. 3600–3500 Ma, 3400–3300 Ma and 3250–3150 Ma (Guitreau et al., 2017; Jayananda et al., 2015, 2023). Directly south of Holenarsipur, in the Sargur region U–Pb zircon ages of gneisses reveal ca. 3400–3100 Ma (Bidyananda et al., 2016). Further, North and Northeast TTG-type granitoids from the Shimoga—western margin of the Chitradurga greenstone belt provide U–Pb zircon ages ca. 3300–3100 Ma (Jayananda et al., 2019; Ravindran et al., 2023 and reference therein). U–Pb zircon ages coupled with whole rock Nd isotope data and *in-situ* Hf isotope data of zircon reveal widespread TTG-type granitoid magmatic accretion corresponding to high rates of continental growth during ca. 3400–3300 Ma and ca. 3250–3150 Ma with minor preserved crust accreted ca. 3600–3500 Ma (see supplementary figure S17; Guitreau et al., 2017; Jayananda et al., 2015, 2023 and reference therein). Sm–Nd whole rock isochrons of komatiite to basalts and U–Pb zircon ages of felsic volcanic flows of the interlayered Sargur Group volcanic rocks reveal ages of ca. 3400, ca. 3350 Ma, ca. 3200 Ma, 3150 Ma (Jayananda et al., 2023 references therein). Further detrital zircons from Sargur Group sedimentary assemblages also provide ages ranging ca. 3600–3150 Ma with major peaks around ca. 3400–3300 Ma and 3250–3150 Ma with minor peaks ca. 3600–3500 Ma (see supplementary figure S17, Mitra et al., 2023; Harshitha et al., 2024 and references therein). Consequently, published ages of granitoids, volcanics and sedimentary assemblages from the WDC reveal major episodes crust formation with high rates of episodic continental growth in the WDC during ca. 3600–3500 Ma, ca 3400–3300 Ma and ca. 3250–3150 Ma.

9.3 Thermal and chemical evolution of Archean mantle

Archean greenstone volcanics are considered as windows into the mantle. Heat flow models on the Archean Earth indicate higher heat production associated with rapid decay of short lived as well as long lived radiogenic elements resulting in steeper geothermal gradients 2 to 3 times higher than modern geothermal gradients. Elemental and radiogenic isotope data of those volcanics provide invaluable insights into thermal and chemical evolution of Archean mantle through time. Field evidence such as flow top breccias/pillow breccia, spinifex textures coupled with high MgO (20–43 wt%) and MgO versus FeO plot (see supplementary figure S4, refer Jayananda et al., 2016) of ca. 3400–3150 Ma komatiites and komatiite basalts reveal magma generation through high degree melting (45–50%) of deep mantle and erupted at 1600–1760 °C, and temperature of the melts were still higher (∼100 °C) at place of their origin (Jayananda et al., 2016). The low incompatible element contents particularly low to moderate REE concentrations (0.38–36.28 ppm), coupled with Nd isotopes [($\varepsilon Nd_{(T)}$ = 0 to +5)] depict heterogeneous deep mantle reservoirs ranging depleted deep mantle (Jayananda et al., 2008, 2023). The long-term depletion history of deep mantle which could be possibly link to an earlier differentiation through plume possibly during 3800–3600 Ma (Jayananda et al., 2008, 2023). Furthermore, Nd [(εNd_T = 0 to 4)] and Hf [(εHf_T = 0 to 6)] isotope data (except few negative εNd values) of contemporaneous (ca. 3400–3200 Ma) TTGs (Jayananda et al., 2023) also consistent with their derivation from shallower depleted mantle with minor involvement pre-existing continental crust. Such depleted signatures in turn imply differentiation of shallower mantle during an earlier differentiation contributing to continental growth. Consequently, the depletion of shallow and deep depleted mantle reservoirs implies an earlier event of shallow and deep mantle melting contributing to an earlier episode of continental growth in the form of TTG-komatiite magmatism prior to ca. 3600 Ma (Jayananda et al., 2023).

9.4 Archean sedimentary assemblages: Provenance and tectonic context of sedimentary basin development

Archean sedimentary assemblages form key archives to address surface environments, redox conditions of ocean-atmospheric system, microbial activity and oxygenation of oceans. The preserved sedimentary record from different stratigraphic units in the western Dharwar craton form a wide time window (ca. 3300–2600 Ma) to evaluate the sedimentary environments including redox conditions, oxygenation, origin of BIFs and tectonic context of basin development through time. The dominant sedimentary sequences in the Sargur Group comprises quartzite, pelite, carbonates and BIFs, which affected by variable degree of deformation and amphibolite to granulite facies metamorphism (Jayananda et al., 2013; Mukherjee et al., 2025). Detrital zircons from quartzite and metapelites provided ca. 3600–3150 Ma for their provenance (Mitra et al., 2023 and references therein). The sedimentary sequences such as quartzites, metapelites and carbonates probably deposited shallow shelf environments. No major study initiated on the elemental and isotopic characteristics of the sedimentary sequences of

Sargur Group. The tectonic environment in which the sediments deposited is poorly known in view of strong deformation and polymetamorphic history. However, associated lithological sequences such as older TTGs, komatiites their deposition in shallow shelf adjacent to a microcontinent or oceanic plateau or in oceanic arc environment (Jayananda et al., 2023). The Bababudan Group represents intracratonic basin developed on the continental crust and contain shallow to deep water sediments including oligomictic conglomerate sitting on a paleosol, intermittent layers of cross-bedded quartzites in mafic volcanic flows, phyllites and thick BIFs. Elemental and isotopic data on these sedimentary sequences are poorly known. Published detrital U–Pb zircon ages reveal ca. 3600–3070 Ma for their provenance (Mallens et al., 2023; Mitra et al., 2023). The tectonic context of development Bababudan Group basins attributed to sagduction (Chardon et al., 1998), a failed rift (Sreehari et al., 2021), plume-arc setting (Manikyamba et al., 2021). Detailed tectonic fabrics mapping and kinematic analysis of Bababudan basin and adjacent basement reveal basin development on the old basement linked to the unique tectonic regime in the interior of the Archean craton driven by mantle upwelling caused by slab break off associated with collision at 3100 Ma (Mallens et al., 2023) and eruption of dense volcanic traps on the basement and thermal blanketing of continental crust (Chardon et al., 1998).

The sedimentary sequences in the Chitradurga Group like polymict Talya conglomerate, minor intraformational conglomerate (K.M Kere), thick carbonate (stromatolitic), greywacke-argillite-carbonaceous shale-BIFs units. These sedimentary sequences from WSW (siliciclastics–stromatolitic carbonate) to ENE (greywacke-argillite-carbonaceous shales-BIFs) reveal a progressive deepening of the basin. Detrital U–Pb zircon ages reveal their provenance evolved in successive stages during 3500–3400 Ma, 3350–3300 Ma and 3200–3100 Ma, 3000–2900 Ma and 2700–2500 Ma (Khelen et al., 2020; Krapez et al., 2020; Harshitha et al., 2024). Published ages on volcanism, granitoids and detrital zircon ages reveal opening of basin started ca. 2740 Ma and closer of the basin during 2560–2500 Ma (Jayananda et al., 2013; Krapez et al., 2020). The tectonic context of Chitradurga basin is debated and various models have been presented including back-arc basin (Chadwick et al., 2000), back-arc basin with an east facing continental arc (Jayananda et al., 2013; Krapez et al., 2020). Elemental, radiogenic Nd (see supplementary figure S3) and oxygen isotope data on the Neoarchean carbonate rocks from Chitradurga greenstone belt indicate their derivation from mixed provenance involving ancient continental crust as old as 3500 Ma and younger juvenile sources originated from long term depleted mantle (Govind et al., 2021).

The Shimoga basin preserve sedimentary sequences including carbonate, chert-greywacke-argillite-carbonaceous shale-BIFs sequences. Besides polymict conglomerate found along the eastern boundary of the basin where large boulders to pebbles are dumped rapidly into a newly opened rift system. Sedimentology of these sequences and tectonic context of basin development is poorly known. However, distribution of these sequences indicates from a failed rift to continental arc environment depicting deepening of basin to the north to northeast. Elemental and isotope data of sedimentary assemblages is poorly known. The sedimentary sequences interlayered with basaltic volcanics in the lower levels and felsic volcanics in the higher stratigraphic levels. Sm–Nd whole rock isochron yield 2638 ± 66 Ma for mafic to intermediate volcanics (Giri et al., 2019) whilst U–Pb zircon ages indicate 2605 ± 5 Ma for pyroclastic felsic volcanics (Nutman et al., 1996). The basin appears to be closed through collision with Bababudan Group as revealed by the intrusion of Koppa granite at 2590 Ma. The sediments interlayered mafic volcanics appears to be deposited during 2638–2590 Ma.

The Dharwar basin is the youngest volcano-sedimentary basin and interpreted as foreland basin (Chadwick et al., 2000). The basin comprises subordinate mafic to felsic volcanics and voluminous sedimentary assemblages from WSW to ENE including platform carbonates, greywacke-argillite-BIFs and intraformational conglomerates without any framework support imply deepening of basin. Elemental ratios of greywacke-argillite suggest their derivation from mixed provenance involving pre-existing basement granitoids and newly formed volcanic arcs (Ugarkar et al., 2017) and deposited in a continental arc setting.

9.5 Redox conditions of Archean surface environments, oxygenation of oceans and emergence of biosphere

The interplay of geological, chemical and biological processes that drives the oxygenation of oceans-atmosphere is fundamental to emergence of Earth's biosphere and habitable continents. The signatures of redox sensitive isotope tracers (Fe, N and S) in the Archean sedimentary record provide invaluable insights on surface environments, redox recycling and metabolic pathways of biological activity (Thomazo et al., 2009). Geological evidence together with redox sensitive elemental and isotope biomarkers reveal Great Oxygenation Event (GOE) with free oxygen on the ocean surface and atmosphere occurred close to 2.4 billion years (Bekker et al., 2004). On the contrary few workers (e.g. Anbar et al., 2007) argued that transient oxygenation of ocean and atmosphere occurred much earlier at least few hundred million years. Despite numerous contributions on the tectonostratigraphic framework and evolution of continental crust in the Dharwar craton (e.g. Krapez et al., 2020) but only few studies addressed redox conditions and oxygenation of oceans-atmosphere

through Archean (e.g., Hashizume et al., 2016; Mishima et al., 2017). The preserved sedimentary profiles from different stratigraphic units (Sargur Group and Dharwar Supergroup) in the western Dharwar craton form wide time window (ca. 3300–2600 Ma) to address the redox conditions of Archean ocean-atmospheric system. Few recent multi-disciplinary studies on WDC have addressed the sedimentary environments and redox conditions of ocean-atmospheric system, oxygenation and microbial activity (Hashizume et al., 2016; Mishima et al., 2017; Sindhuja et al., 2022; Mukherjee et al., 2025). Recent mineralogic and redox sensitive elemental data (lack of Ce anomalies, higher SiO_2 and Fe_2O_3) on the Sargur Group BIFs consistent with their origin in anoxic environments wherein iron dissolved in ocean (Mukherjee et al., 2025). The Bababudan Group corresponds to lower part of the Dharwar Supergroup preserve thick BIFs which confined to highest stratigraphic levels. The different facies of BIFs (oxide, sulphide, carbonate and silicate facies) coupled with variable Ce anomalies (without Ce anomalies but few samples showing negative Ce anomalies) argue for dominant anoxic conditions with periodic availability of minor oxygen on oceanic surface (Mukherjee et al., 2025). This observation is in consistent with isotope biomarker data using Fe–N isotopes on ca. 2720 Ma BIFs (Hashizume et al., 2016) which showed fluctuations in oxygen production on the ocean surface linked to microbial activity during the beginning of Neoarchean at least 300 Ma prior to the Great Oxidation Event.

The Chitradurga basin preserves spectacular stromatolites along its western margin (near Bhimasandra) reflect intermittent microbial activity with minor oxygen availability in the shallow shelf environment. Thick carbonate sequences immediately 50 km south in Dodguni region exhibit depleted oxygen isotope signatures (^{18}O −13.51‰ VPDB to −8.46‰ VPDB) suggest higher sea water temperatures (Khelen et al., 2019) during their precipitation 2639 ± 32 Ma (Russell et al., 1996). The variable Ce anomalies including negative or absence of Ce anomalies in BIFs of the Chitradurga basin possibly linked to periodic fluctuations in redox conditions of ocean with traces or without oxygen availability on the ocean surface (Mukherjee et al., 2025).

The Shimoga–Dharwar basin (2636–2600 Ma; Giri et al., 2019; Krapez et al., 2020) is the youngest volcano-sedimentary basin with carbonate platform in the west whilst greywacke-argillite-BIFs often containing abundant sulphides to the east suggest shallow shelf conditions in the west with traces of oxygen and progressively deeper anoxic environments to the east. Redox sensitive elemental data [Ce (Ce/Ce* = 0.45–0.82)] of BIFs consistent with transient environments from anoxic to traces of oxygen on the ocean surface at the dawn of Great Oxidation Event (Mukherjee et al., 2025).

The sulphur–Mass Independent Fractionation (S-MIF) study of sulphides from the Dharwar Supergroup reveal a change in atmospheric chemistry from lower stratigraphic level to upper stratigraphic level through Archean (Mishima et al., 2017) with the first appearance of oxygen at the end of Neoarchean. Furthermore, the wide range of S-MIF data on the lower stratigraphic level of Dharwar Supergroup suggest microbial sulphate reduction was active in the low sulphate environment (Mishima et al., 2017).

To summarize, mineralogic data coupled with redox sensitive elements and isotope tracers on the preserved sedimentary sequences of oldest to youngest stratigraphic units reveal anoxic through transient environments with traces of oxygen on the ocean surface at the end of Archean.

9.6 Tectonics of the Archean earth (3500–2600 Ma) and building of habitable continent

Tectonics of the Archean earth is one of the most debated topics in Earth and Planetary Sciences. Despite numerous studies addressed the tectonics of the early earth, formation of continental crust and craton building mechanisms but there is no consensus among the scientific community (Nebel et al., 2024 and references therein). Models involving uniformitarian, non-uniformitarian, transient tectonics and crustal drips have been proposed (e.g., Jayananda et al., 2023). The WDC preserve large tilted crustal profile with more than a billion-year crustal history from ca. 3600–2500 Ma form a wide tectonic window into Archean earth (Guitreau et al., 2017; Jayananda et al., 2013, 2023). Several models invoking vertical tectonics (Chardon et al., 1996, 1998), horizontal tectonics (Chadwick et al., 2000), combined plume-arc model (Jayananda et al., 2018, 2023). Most of the models are based on petrologic and elements whilst few models are based on tectonic fabrics, petrologic, isotopic ages and elemental data (Jayananda et al., 2023 and references therein). The WDC preserve Archean granitoid–greenstone assemblages including ca. 3600–3200 Ma TTG-type granitoids, ca. 3150 Ma Chikmagalur granodiorite, ca. 3000–2950 Ma and ca. 2600 Ma potassic granites with associated three cycles of volcanism ca. 3400–3200 Ma komatiite dominated greenstones, ca.3000–2720 Ma Basaltic to felsic volcanics and ca. 2700–2600 Ma basaltic to felsic volcanics and interlayered sediments deposited from ca. 3300–3100 Ma, 2900–2700 Ma, 2650–2560 Ma. The oldest preserved crust in the cratonal core in WDC comprises TTG-type granitoids and komatiite to high-Mg basaltic flows both of which have intruded by diapiric trondhjemite plutons. Any tectonic model proposed should explain the evolving rock compositions, fabrics and metamorphic record from through 3600–2600 Ma. Geochronologic data coupled with elemental and isotope data reveal dominant komatiite volcanism and associated Na-rich granitoids of TTG affinity

during ca. 3400–3200 Ma whilst amygdular to vesicular basalts ca. 3000–2850 Ma and 2700–2600 Ma basalt-intermediate to felsic volcanics of arc affinity. There is progressive decrease of MgO and other compatible elements (Ni and Cr) in volcanics (komatiites to boninite-basalts) during 3400–2600 Ma reflecting decrease of mantle temperature, degree and depth of melting which in turn spatially linked to a possible transition high degree melting in deep mantle in hotspot/plume settings during 3400–3300 Ma to shallower melting in arc settings. Furthermore, the granitoids (TTGs to sanukitoids) also show secular changes in composition from Na_2O rich to CaO and K_2O which attributed to shallower melting within plagioclase stability field under higher geothermal gradients during 3600–3400 Ma whilst slightly deeper melting within or beneath plagioclase stability field during 3300–3200 Ma (Jayananda et al., 2018, 2023). In contrast transitional TTGs and juvenile granitoids of sanukitoid affinity originated by melting deeper arc crust and/or arc mantle beneath plagioclase stability field accounting higher CaO and K_2O (Jayananda et al., 2018). Tectonic fabric mapping and kinematic analysis of 3600–3200 Ma granitoids–greenstone assemblages reveal dome-keel structures developed through gravitational collapse of high density volcanics into granitoid basement in hotspot environments whilst 3000–2850 Ma volcanics forming sagducting ridges on the old basement (Chardon et al., 1996, 1998) whilst 2700–2600 Ma greenstone basins form typical arc (back arc or continental arcs; Chadwick et al., 2000; Jayananda et al., 2013). Recent multidisciplinary study reveal distinct tectonic units in the cratonal core including Paleoarchean (ca. 3400 Ma) oceanic plateau fragments, oceanic arcs, oceanic ridge and a (>3600–3500 Ma) microcontinent and all these tectonic units assembled through horizontal motion of intervening oceanic crust at ca. 3200 Ma (Jayananda et al., 2023). The ca. 3000–2720 Ma Bababudan Group intra-cratonic volcano-sedimentary basin has been attributed to sagduction (Chardon et al., 1996, 1998) or a failed rifts (Sreehari et al., 2021) or plume-arc setting (Manikyamba et al., 2021). The failed rift model (Sreehari et al., 2021) to explain the sedimentary assemblages like oligomict conglomerate and cross-bedded quartzite whilst plume-arc model (Manikyamba et al., 2021) not supported by tectonic fabrics data and metamorphic record whilst tectonic fabric data including kinematic analysis reveal downward displacement of high-density greenstone load (sagduction) into the basement in the context of rising mantle hotspot (Chardon et al., 1998). On contrary the bimodal volcanics of ca. 2700–2600 Ma Chitradurga and Shimoga–Dharwar basin show typical arc signatures originated in back-arc or continental arc settings (Chadwick et al., 2000).

Archean potassic granite plutons form key archives for our understanding of crustal reworking processes, continental collision and cratonization. In the WDC three generation of potassic granites i.e. ca. 3150 Ma Chikmagalur granite, ca. 3000–2950 Ma Bellur–Nagamangala, Hosadurga and Bukkapatna granites and ca. 2620–2600 Ma Chitradurga granite. These ca. 3150 Ma funnel shaped Chikmagalur granite (Jayananda et al., 2015) is the oldest pluton that intrude the basement North-west of Holenarsipur greenstone belt and runs northward form the base for the Bababudan basin. U–Pb zircon ages of TTGs on either side of the granitoids and detrital zircons from oligomictic conglomerate above granite reveal a possible continental collision causing thickening and remelting of lower crust leading to Chikmagalur granite emplacement ca. 3150 Ma (Mallens et al., 2023) and subsequent emergence of continental landmass above sea level close to 3000 Ma as revealed by paleosol at the contact between Chikmagalur granite and oligomict conglomerate at the base of Bababudan basin (Srinivasan and Ojakangas, 1986). The ca. 3000–2950 Ma high-potassic Bellur–Nagamangala plutons emplaced the Sargur Group Nagamangala greenstone belts and adjoining TTG-type gneisses probably corresponding to assembly of two tectonic units through collision close to 3000 Ma (Jayananda et al., 2019) which substantiated by high pressure assemblages. On the other hand, the ca. 2600 Ma Chitradurga granite located in between Chitradurga and Javagondanahalli greenstone belts which are bounded by transpressional shear zone. This granite shows characteristics of A-type granite which probably originated during assembly of these Chitradurga and Javagondanahalli arcs through collision. The tectonic evolution of the Archean continental crust involves plume impact that produce oceanic volcanic plateaus, lateral motion of intervening oceanic crust initiation leads to development of arcs, collision of arcs with plateaus/old continental fragments produce trondhjemite plutons, collision of small microcontinental blocks with slab breakoff produce hotspot which drive A-type granite magmatism during ca. 3150 Ma 3000 Ma and 2600 Ma.

In summary, the potassic granites in the Western Dharwar craton suggest three stages of stabilization of continental crust through three stages ca. 3150–3100 Ma, 3000–2950 Ma, ca. 2600 Ma leading to formation larger landmass. Emergence of continent above the sea level revealed by a ca. 3000 Ma paleosol at the base of Bababudan basin at the contact between basement and oligomict conglomerate suggest continental weathering above sea level in the presence of minimal oxygen. Rising continents above sea levels ca. 3000 Ma, weathering and sediment input contributed nutrient supply to the oceans. Redox sensitive elements and isotope biomarkers (^{56}Fe and ^{15}N) reveal microbial activity caused periodic fluctuation in oxygen production on ocean surface, iron and carbonate recycling (Hashizume et al., 2016) which in consistent with S-MIF data indicating change in atmospheric chemistry from Meso-to Neoarchean (Mishima et al., 2017). Furthermore,

ca. 2650 Ma algal mats in carbonates (stromatolites) from the Chitradurga basin reveal microbial activity in shallower shelf environments and oxygenation of oceans at the dawn of the Great Oxygenation Event (Hashizume et al., 2016; Khelen et al., 2019; Govind et al., 2021; Harshitha et al., 2024). This followed by collision of the micro-blocks close to 2500 Ma leading to final cratonization and establishment of larger stable continental mass hosting early habitats of life marks the end of Archean.

10 Conclusions

The conclusions of the present synthesis can be summarized as follows.

1. The felsic continental crust in the western Dharwar craton differentiated from mantle in successive stages during ca. 3600–3500 Ma, 3440–3350 Ma, 3330–3270 Ma and 3200–3150 Ma and witnessed major reworking events leading to emplacement of potassic plutons during ca. 3150 Ma, ca. 3000–2950 Ma and ca. 2600 Ma and stabilization of Archean crust.

2. The tectonic fabrics data coupled with sedimentary assemblages in the older Sargur Group and younger Dharwar Supergroup reveal that older greenstone basins developed in the oceanic region as oceanic plateaus in hotspot environments rising plume and oceanic arcs whilst Dharwar Supergroup basin (Bababudan) formed as intracratonic basins on the stabilized basement associated with mantle upwelling causing emplacement of dense volcanic traps. Finally, the younger basins (Chitradurga and Shimoga–Dharwar) developed in arc settings (back arc/continental/oceanic arcs).

3. Redox sensitive elements and isotope biomarkers of carbonates and BIFs reveal dominantly anoxic environments prior to ca. 3000 Ma whilst fluctuating surface environments with periodic shift from anoxic to oxic conditions on ocean surface associated with microbial activity.

4. Collision of arcs with micro-continent with eventual amalgamation of micro-blocks lead to the formation of larger continental landmass above sea levels, shifting of nutrients to oceans and microbial activity leading formation habitable continent hosting early habitats of life at the dawn of the GOE.

Acknowledgements

We thank Prof. M. Santosh for inviting to contribute this review synthesis. This work is supported by Sir J.C. Bose National Fellowship grant awarded to M. Jayananda. We thank two anonymous reviewers for their insightful reviews and Dr. Vasanthi for efficient editorial handling.

Declaration of competing interest

The authors declare that they have no known competing financial interests or personal relationships that could have appeared to influence the work reported in this review synthesis.

Supplementary material

Supplementary information for this article can be found online at https://doi.org/10.63335/j.hp.2025.0016.

CRediT authorship contribution statement

K.R. Aadhiseshan: Writing—review, data processing, and editing

M. Jayananda: Conceptualization, Writing—original draft, Project administration, Investigation, Funding acquisition.

References

Aldanmaz, E., Pearce, J.A., Thirlwall, M.F., Mitchell, J.G., 2000. Petrogenetic evolution of late Cenozoic, post-collision volcanism in western Anatolia. Turkey. Journal of Volcanology and Geothermal Research 102, 67–95. doi:10.1016/S0377-0273(00)00182-7.

Anbar, A.D., Duan, Y., Lyons, T.W., Arnold, G.L., Kendall, B., Creaser, R.A., Kaufman, A.J., Gordon, G.W., Scott, C., Garvin, J., Buick, R., 2007. A whiff of oxygen before the great oxidation event? Science 317, 1903–1906. doi:10.1126/science.1140325.

Bedard, J.H., 2018. Stagnant lids and mantle overturns: implications for Archaean tectonics, magma genesis, crustal growth, mantle evolution, and the start of plate tectonics. Geoscience Frontiers 9, 19–49. doi:10.1016/j.gsf.2017.01.005.

Bekker, A., Holland, H.D., Wang, P.-L., Rumble III, D., Stein, H.J., Hannah, J.L., Coetzee, L.L., Beukes, N.J., 2004. Dating the rise of atmospheric oxygen. Nature 427, 117–120. doi:10.1038/nature02260.

Bidyananda, M., Gerdes, A., Goswami, J.N., 2016. U-Pb and Hf isotope records in detrital and magmatic zircon from Eastern and western Dharwar Craton, southern India: evidence for coeval Archean crustal evolution. Precambrian Research 275, 496–512. doi:10.1016/j.precamres.2016.01.009.

Chadwick, B., Ramakrishnan, M., Viswanatha, M.N., 1985. Bababudan a late Archaean intracratonic volcano-sedimentary basin, Karnataka. Southern India. Journal of the Geological Society of India 26, 769–821. doi:10.17491/jgsi/1985/261101.

Chadwick, B., Vasudev, V.N., Hegde, G.V., 2000. The Dharwar craton, southern India, interpreted as the result of Late Archaean oblique convergence. Precambrian Research 99(1-2), 91–111. doi:10.1016/S0301-9268(99)00055-8.

Chardon, D., Choukroune, P., Jayananda, M., 1996. Strain patterns, de'collement and incipient sagducted greenstone terrains in the Archaean Dharwar craton (south India). Journal of Structural Geology 18, 991–1004. doi:10.1016/0191-8141(96)00031-4.

Chardon, D., Choukroune, P., Jayananda, M., 1998. Sinking of the Dharwar basin (South India): implications for Archaean tectonics. Precambrian Research 91(1-2), 15–39. doi:10.1016/S0301-9268(98)00037-0.

Chardon, D., Jayananda, M., Chetty, T.R.K., Peucat, J.-J., 2008. Precambrian continental strain and shear zone patterns: the South Indian

case. Journal of Geophysical Research 113, B08402. doi:10.1029/2007JB005299.

Chardon, D., Jayananda, M., Peucat, J.-J., 2011. Lateral constrictional flow of hot orogenic crust: insights from the Neoarchean of south India, geological and geophysical implications for orogenic Plateaux. Geochemistry Geophysics Geosystems 12, Q02005. doi:10.1029/2010GC003398.

Corfu, F., Hegde, V.S., 2020. U–Pb systematics of the western Dharwar Craton - Glimpses of a billion-year history of crustal evolution and relations to ancient supercratons. Journal of South American Earth Sciences 102, 102659. doi:10.1016/j.jsames.2020.102659.

Dasgupta, A., Bhowmik, S.K., Dasgupta, S., Avila, J., Ireland, T.R., 2019. Mesoarchaean clockwise metamorphic PT path from the Western Dharwar Craton. Lithos 342, 370–390. doi:10.1016/j.lithos.2019.06.006.

Fedo, C.M., Wayne Nesbitt, H., Young, G.M., 1995. Unraveling the effects of potassium metasomatism in sedimentary rocks and paleosols, with implications for paleoweathering conditions and provenance. Geology 23(10), 921. doi:10.1130/0091-7613(1995)023<0921:UTEOPM>2.3.CO;2.

Giri, A., Anand, R., Balakrishnan, S., Dash, J.K., Sarma, D.S., 2019. Neoarchean magmatism in Shimoga greenstone belt, India: evidence for subduction-accretion processes in the evolution of the western Dharwar stratigraphy. Lithos 330–331, 177–193. doi:10.1016/j.lithos.2019.02.015.

Govind, A.V., Behera, K., Dash, J.K., Balakrishnan, S., Rajneesh, B., Shreyas, M., Srinivasan, R., 2021. Trace element and isotope Geochemistry of Neoarchean carbonate rocks from the Dharwar craton, southern India: implications for depositional environments and mantle influence on ocean chemistry. Precambrian Research 357, 106137. doi:10.1016/j.precamres.2021.106137.

Guitreau, M., Mukasa, S.B., Loudin, L., Krishnan, S., 2017. New constraints on the early formation of the Western Dharwar Craton (India) from igneous zircon U-Pb and Lu-Hf isotopes. Precambrian Research 302, 33–49. doi:10.1016/j.precamres.2017.09.016.

Harshitha, G., Manikyamba, C., Santosh, M., Yang, C.-X., Krishna, A.K., Sai, V.V.S., Reddy, I.P., 2024. Paleo-Mesoarchean sedimentary record in the Dharwar Craton, India: implications for Archean Ocean oxygenation. Geoscience Frontiers 15, 101701. doi:10.1016/j.gsf.2023.101701.

Hashizume, K., Pinti, D.L., Orberger, B., Cloquet, C., Jayananda, M., Soyama, H., 2016. A biological switch at the ocean surface as a cause of laminations in a Precambrian iron formation. Earth and Planetary Science Letters 446, 27–36. doi:10.1016/j.epsl.2016.04.023.

Jayananda, M., Aadhiseshan, K.R., Kusiak, M.A., Wilde, S.A., Sekhamo, K.U., Guitreau, M., Gireesh, R.V., 2020. Multi-stage crustal growth and Neoarchean geodynamics in the Eastern Dharwar Craton, southern India. Gondwana Research 78, 228–260. doi:10.1016/j.gr.2019.09.005.

Jayananda, M., Chardon, D., Peucat, J.J., Fanning, C.M., 2015. Paleo- to Mesoarchean TTG accretion and continental growth in the western Dharwar craton, Southern India: constraints from SHRIMP U–Pb zircon geochronology, whole-rock geochemistry and Nd–Sr isotopes. Precambrian Research 268, 295–322. doi:10.1016/j.precamres.2015.07.015.

Jayananda, M., Duraiswami, R.A., Aadhiseshan, K.R., Gireesh, R.V., Prabhakar, B.C., Kafo, Kowe-u, Tushipokla, Namratha, R., 2016. Physical volcanology and geochemistry of Paleoarchean komatiite lava flows from the western Dharwar craton, southern India: implications for Archaean mantle evolution and crustal growth. International Geology Review 58-13, 1569–1595. doi:10.1080/00206814.2016.1172350.

Jayananda, M., Guitreau, M., Aadhiseshan, K.R., Miyazaki, T., Chung, S.L., 2023. Origin of the oldest (3600–3200 Ma) cratonic core in the Western Dharwar Craton, Southern India: implications for evolving tectonics of the Archean Earth. Earth-Science Reviews 236, 104278. doi:10.1016/j.earscirev.2022.104278.

Jayananda, M., Kano, T., Peucat, J.J., Channabasappa, S., 2008. 3.35 Ga komatiite volcanism in the western Dharwar craton, southern India: constraints from Nd isotopes and whole-rock geochemistry. Precambrian Research 162(1-2), 160–179. doi:10.1016/j.precamres.2007.07.010.

Jayananda, M., Martin, G., Tarun Thomas, T., Martin, H., Aadhiseshan, K.R., Gireesh, R.V., Peucat, J.-J., Satyanarayanan, M., 2019. Geochronology and geochemistry of Meso- to Neoarchean magmatic epidote-bearing potassic granites, Western Dharwar Craton (Bellur–Nagamangala–Pandavpura corridor), Southern India: implications for the successive stages of crustal reworking and cratonization, in: Dey, S., Moyen, J.-F. (Eds.), Archean Granitoids of India: Windows into Early Earth Tectonics. Geological Society, London, Special Publications. volume 489. doi:10.1144/SP489-2018-125.

Jayananda, M., Santosh, M., Aadhiseshan, K.R., 2018. Formation of Archean (3600–2500 Ma) continental crust in the Dharwar Craton, southern India. Earth-Science Reviews 181, 12–42. doi:10.1016/j.earscirev.2018.03.013.

Jayananda, M., Tsutsumi, Y., Miyazaki, T., Gireesh, R.V., Kapfo, K.U., Hidaka, H., Kano, T., 2013. Geochronological constraints on Meso- and Neoarchean regional metamorphism and magmatism in the Dharwar craton, southern India. Journal of Asian Earth Sciences 78, 18–38. doi:10.1016/j.jseaes.2013.04.033.

Kaempf, J., Clark, C., Johnson, T.E., Jayananda, M., Julian, A., Payne, J., Sajeev, K., Martin, H., 2025. Archean polymetamorphism in the Central Dharwar Craton, Southern India. Journal of Metamorphic Petrology 43(1), 71–95. doi:10.1111/jmg.12798.

Khelen, A.C., Manikyamba, C., Subramanyam, K.S.V., Santosh, M., Ganguly, S., Kalpana, M.S., Subba Rao, D.V., 2019. Archean seawater composition and depositional environment – Geochemical and isotopic signatures from the stromatolitic carbonates of Dharwar Craton, India. Precambrian Research 330, 35–57. doi:10.1016/j.precamres.2019.04.020.

Khelen, A.C., Manikyamba, C., Tang, L., Santosh, M., Subramanyam, K.S.V., Singh, T.D., 2020. Detrital zircon U-Pb geochronology of stromatolitic carbonates from the greenstone belts of Dharwar Craton and Cuddapah basin of Peninsular India. Geoscience Frontiers 11, 229–242. doi:10.1016/j.gsf.2019.04.010.

Komiya, T., Yamamoto, S., Aoki, S., Sawaki, Y., Ishikawa, A., Tashiro, T., Koshida, K., Shimojo, M., Aoki, K., Collerson, K.D., 2015. Geology of the Eoarchean, N3.95 Ga, Nulliak supracrustal rocks in the Saglek Block, Northern Labrador, Canada: the oldest geological evidence for plate tectonics. Tectonophysics 662, 40–62. doi:10.1016/j.tecto.2015.05.003.

Krapez, B., Srinivasa Sarma, D., Ram Mohan, M., McNaughton, N.J., Rasmussen, B., Wilde, S.A., 2020. Tectonostratigraphy of the Late Archean Dharwar Supergroup, Dharwar Craton, India: defining a tectonic history from spatially linked but temporally distinct intracontinental and arc-related basins. Earth-Science Reviews 201, 102966. doi:10.1016/j.earscirev.2019.102966.

Kumar, A., Bhaskar Rao, Y.J., Sivaraman, T.V., Gopalan, K., 1996. Sm-Nd ages of Archaean metavolcanics of the Dharwar craton, South India. Precambrian Research 80, 205–216. doi:10.1016/S0301-9268(96)00015-0.

Ma, Haitao, Dilek, Y., Lian, D., Cai, P., Jayananda, M., Aadhiseshan, K.R., Yang, J., 2024. Parental magma and mantle source compositions of chromitites in the Mesoarchean Nuggihalli greenstone belt, India: evidence for Archean subduction zone magmatism. Journal of the Geological Society, London 182, 1–12. doi:10.1144/jgs2024-158.

Mallens, J., Guitreau, M., Jayananda, M., Gannoun, A., Fonquerine, C., Voyer, E., Aadhiseshan, K.R., 2023. Detrital zircon evidence for Mesoarchean continental collision in the Western Dharwar craton (India). Goldschmidt abstract. doi:10.7185/gold2023.

Manikyamba, C., Ganguly, S., Santosh, M., Tang, L., Sindhuja, C.S., Pahari, A., Singh, T.D., Saha, A., 2021. Tectonic juxtaposition of plume and subduction derived magmatic sequences in the Bababudan greenstone terrane, western Dharwar Craton, India: constraining crustal accretion processes in a Neoarchean subduction-collision orogeny. Precambrian Research 355, 106097. doi:10.1016/j.precamres.2021.106097.

Mishima, K., Yamazaki, R., Satish-Kumar, M., Ueno, Y., Hokada, T., Toyoshima, T., 2017. Multiple sulfur isotope geochemistry of Dharwar Supergroup, Southern India: late Archean record of changing atmospheric chemistry. Earth and Planetary Science Letters 464, 69–83. doi:10.1016/j.epsl.2017.02.007.

Mitra, A., Dey, S., Das, P., Zong, K., Liu, Y., 2023. Nucleation and growth of western Dharwar Craton: a Paleoarchean to Mesoarchean evolutionary history recorded in sediment geochemistry and detrital zircon U-Pb-Hf isotopes-trace elements. Lithos 448-449, 107148. doi:10.1016/j.lithos.2023.107148.

Mukherjee, A., Jayananda, M., Pritam, N., Aadhiseshan, K.R., Satyanarayanan, M., 2025. Geochemistry and origin of the banded Iron formations (BIFs) from the Western Dharwar craton, southern India: implications for evolving redox conditions of Archean oceans. Geochemistry 85, 126268. doi:10.1016/j.chemer.2025.126268.

Nebel, O., Vandenburg, E.D., Capitanio, F.A., Smithies, R.H., Mulder, J., Cawood, P.A., 2024. Early Earth "subduction": short-lived, off-craton, shuffle tectonics, and no plate boundaries. Precambrian Research 408, 107431. doi:10.1016/j.precamres.2024.107431.

Nutman, A.P., Chadwick, B., Krishna Rao, B., Vasudev, V.N., 1996. SHRIMP U/Pb zircon ages of acid volcanic rocks in the Chitradurga and Sandur groups, and granites adjacent to the Sandur schist belt, Karnataka. Journal of the Geological Society of India 47, 153–164. doi:10.17491/jgsi/1996/470202.

Ojakangas, R.W., Srinivasan, R., Hegde, V.S., Chandrakant, S.M., Srikantia, S.V., 2014. The Talya Conglomerate: an Archean (∼2.7 Ga) glaciomarine formation, Western Dharwar Craton. Southern India. Current Science 106, 387–396. URL: https://www.jstor.org/stable/24099899.

Pearce, J.A., Ernst, R.E., Peate, D.W., Rogers, C., 2021. LIP printing: use of immobile element proxies to characterize Large Igneous Provinces in the geologic record. Lithos 392-393, 106068. doi:10.1016/j.lithos.2021.106068.

Polat, A., 2012. Growth of Archean continental crust in oceanic island arcs. Geology 40, 383–384. doi:10.1130/focus042012.1.

Ravindran, A., Mezger, K., Balakrishnan, S., Berndt, J., Ranjan, S., Upadhyay, D., 2023. Formation of Paleo- to Meso-Archean continental crust in the western Dharwar Craton, India: constraints from U-Pb zircon ages and Hf-Pb-Sr isotopes of granitoids and sedimentary rocks. Chemical Geology 615, 121196. doi:10.1016/j.chemgeo.2022.121196.

Reinhard, C.T., Planavsky, N.J., 2020. Biogeochemical controls on the redox evolution of Earth's oceans and atmosphere. Elements 16, 191–196. doi:10.2138/gselements.16.3.191.

Roberts, N.M.W., Santosh, M., 2018. Capturing the Mesoarchean emergence of continental crust in the Coorg Block, southern India. Geophysical Research Letters 45. doi:10.1029/2018GL078114.

Russell, J., Chadwick, B., Krishna Rao, B., Vasudev, V.N., 1996. Whole rock Pb/Pb isotopic ages of late Archean limestones, Karnataka, India. Precambrian Research 78, 261–272. doi:10.1016/0301-9268(95)00082-8.

Sindhuja, C.S., Manikyamba, C., Saha, S., Narayanan, S., Sridhar, B., 2022. Geochemical and carbon isotopic studies of carbonaceous phyllites from Dharwar craton, India – Reconstruction of Precambrian depositional environment. Precambrian Research 372, 106575. doi:10.1016/j.precamres.2022.106575.

Sreehari, L., Toyoshima, T., Satish-Kumar, M., Takahashi, T., Ueda, H., 2021. Structural and geochemical evidence for a failed rift crustal evolution model in Western Dharwar Craton. South India. Lithos 388–389, 106020. doi:10.1016/j.lithos.2021.106020.

Srinivasan, R., Ojakangas, R.W., 1986. Sedimentology of quartz–pebble conglomerates and quartzites of the Archean Bababudan Group: evidence for early crustal stability. The Journal of Geology 94, 199–214. doi:10.1086/629023.

Swami Nath, Ramakrishnan, M., 1981. Early Precambrian Supracrustals of Southern Karnataka, Memoire 112. Geological Survey of India.

Thomazo, C., Pinti, D.L., Busigny, V., Ader, M., Hashizume, K., Philippot, P., 2009. Biological activity and Earth's surface evolutions: insights from carbon, sulfur, nitrogen and iron stable isotopes in the rock record. Comptes Rendus Palévol 8, 665–678. doi:10.1016/j.crpv.2009.02.003.

Ugarkar, A.G., Chandan Kumar, B., Malapur, M.A., Manuvachari, T.B., Kerr, A.C., 2017. Petrography and geochemistry of Archaean greywackes from the northern part of the Dharwar-Shimoga greenstone belt, western Dharwar craton: implications for nature of provenance. Journal of the Geological Society of India 89, 547–553. doi:10.1007/s12594-017-0643-6.

Wyman, D., 2018. Do cratons preserve evidence of stagnant lid tectonics? Geoscience Frontiers 9, 3–17. doi:10.1016/j.gsf.2017.02.001.